UCLouvain

Donostia International Physics Center

FACULTE DES SCIENCES

Faculté des sciences

Calcium Carbonate Precipitation in Alkaline Silica Gel.

Study of Aragonite Biomorph Morphology.

Auteur : Julien ROBIN

Promoteur : Tom Leyssens (UCLouvain)

Juan Manuel Garcia Ruiz (DIPC)

Lecteur·rices : Koen Robeuns, Patricia Luis Alconero, Olivier Riant

Année académique 2024-2025

Master [120] en sciences chimiques, à finalité approfondie

Acknowledgement

I would like to thank Professor Juan Manuel Garcia Ruiz for giving me the opportunity to work on this exiting project. I would like to thank him for his welcome in his laboratory in San Sebastian and for his guidance during this project.

I would like to thank Professor Tom Leyssens for agreeing to be the co-promoter of this project and allowing it to happen. I would like to thank him as well for his help getting everything I need to work and getting me the access to the machines I needed.

Of course, I would like to thank the Protos team in San Sebastian, for their help in the lab, making sure I have everything I need, and outside the lab, making me discover the local food.

I would like to thank the team from Tom's lab, for their help and welcome, even if I was working on a very different project.

For their help with their respective techniques, I would like to thank Raquel Fernandez, Sabine Bebelman, Brigitte Gerin and Alicia González Segura.

Table des matières

1 Biomorphs

1.1 Definition

Biomorphs are defined as self-organizing abiotic composite materials, made of a crystalline carbonate phase and an amorphous silica phase.[1] The crystalline carbonate is present as nanocrystals, aggregating following some long-range order, with the particularity of not following the crystalline habitus of the carbonate. Instead, they form lifelike structures, such as sheets with curved edges, helixes, cones and more. Thus far, the biomorph-forming carbonates that have been reported are Witherite (Barium Carbonate), Monohydrocalcite (Monohydrated Calcium Carbonate), Aragonite (Calcium Carbonate) and Strontianite (Strontium Carbonate).

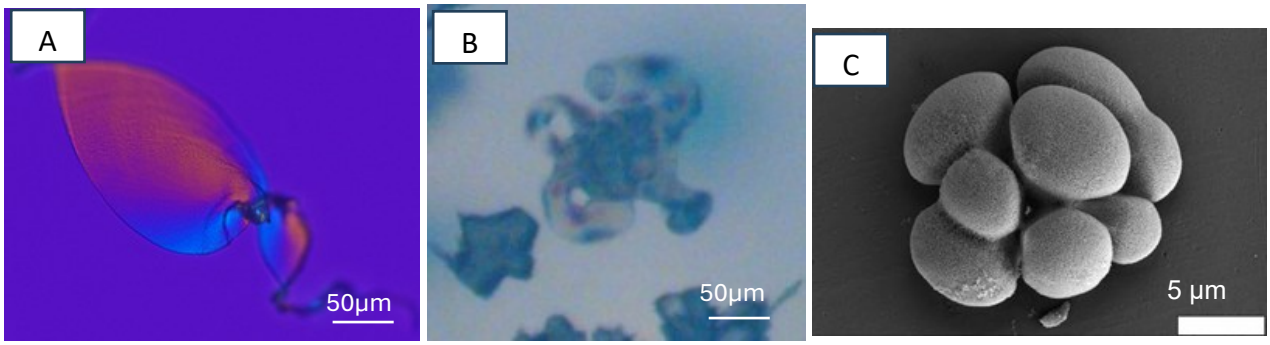

Figure 1 Examples of Biomorphs: A: optical image of a Barium carbonate biomorph, B: optical image of a Calcium carbonate biomorph, C: SEM image of a Barium Carbonate biomorph[2]

1.2 Interest

One of the main interests in studying biomorphs is linked to the study of the apparition of life. Since biomorphs show forms reminiscent of those produced by living organisms, the ability to accurately differentiate a biomorph structure from a fossil of an early organism is crucial for anyone looking to determine when life has appeared on Earth. This raises the question of whether the conditions of the early Earth, the period we estimate conditions allowed for the formation of life, were compatible with the conditions to form biomorphs. Studies of the Hadean Zircon, the oldest surviving crustal material (-4.6Ga to 4Ga) from the Jack Hills[3] puts the formation of an ocean of liquid water at around -4.3Ga, around 800 million years before the first evidence of life. This liquid water was in contact with the primordial crust, containing silica rich material (residual peridite). This led to intense serpentinization, producing gases such as ammonia and methane when N_2 is present, which was one of the main components of the Hadean atmosphere,[4 and still is today. This, in turn, results in a more basic ocean, allowing for the dissolution of more silica, creating the perfect environment for biomorphs: an alkaline silica rich solution, in which CO_2 can dissolve, allowing for the precipitation of carbonates.

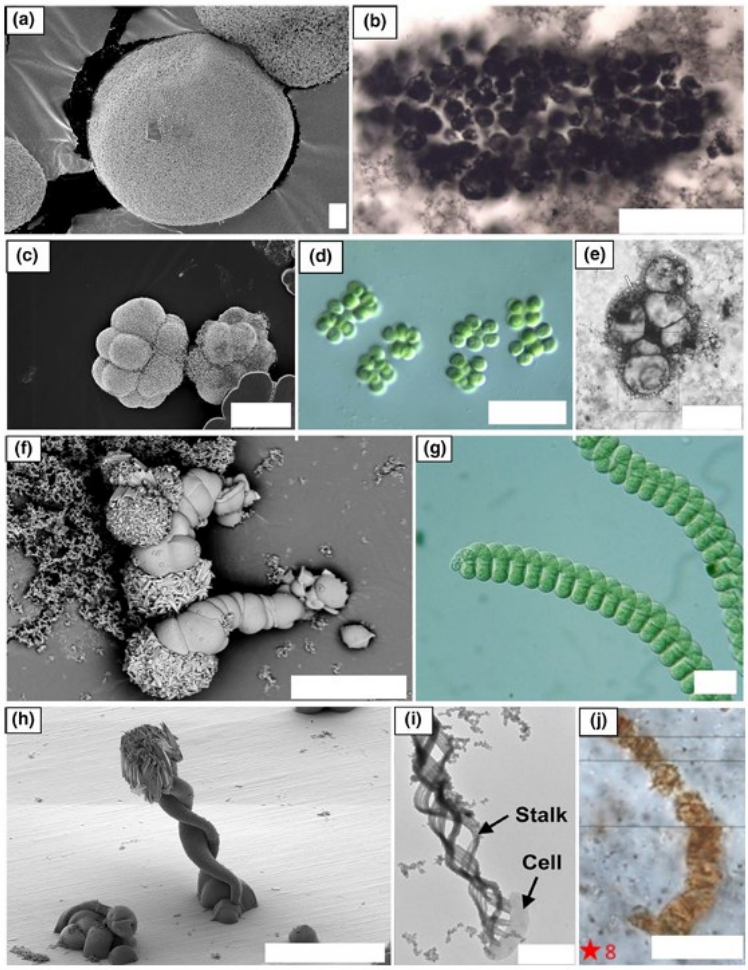

Figure 2 Morphological comparison of specific biomorph shapes, bacteria (or bacteria- related structures) and Archean microstructures. (a) spheroidal biomorph, (b) population of spheroids from the Strelley Pool Formation, (c) framboidal biomorphs, (d) cluster of Microcystis flosaquae, (e) cluster of spheroids from the Strelley Pool formation, (f) wormlike biomorphs, (g) Spirulina sp. (h) helical braid- like biomorph, (i) helical stalks produced by Mariprofundus ferrooxydans, (j) filamentous structures from Apex Chert. Sources of the pictures: (a), (c), (f), (h) this study. (b), (e) Sugitani et al. (2015). (d), (g) Pictures by Pr. Tsukii, Protist Information Server. (i) Singer et al. (2011). (j) Wacey et al. (2015). Scalebars: (a), (i) 1 µm; (b), (d), (e), (f), (g), (h) 50 µm; (c), (j) 10 µm. Figure reproduced from ref [5]

Due to their biomimetic nature, biomorphs could also be the bridging step between classical mineralisation and bio-mineralisation of carbonates. Biomorphs could have been instrumental in the separation of chemical processes, acting like a proto cell. The study of their formation and how they interact with organic molecules then becomes important. It has been shown that biomorphs can be functionalised by using alkoxysilanes[6]. This led to biomorphs integrating the organic molecules in the silica layers. The functionalisation was done by two different methods: during the growth and post-functionalisation. For the first method, the silica source used are tetraethoxysilanes (TEOS) instead of an inorganic silica solution. The TEOS is hydrolysed in water, releasing silica ions, which can be used to grow biomorphs. By replacing a part of the TEOS by functionalised silanes, it is possible to introduce a variety of functional organic groups such as alcohols, amines or fluorescent groups (Figure 3). For the second method, the biomorphs are grow first, then harvested. It is expected that those biomorphs present free silanol groups on their surface, which can be modified by

classical siloxane chemistry (figure 4). In both cases, a wide variety of functional groups can be attached to biomorphs. The main difference between the two techniques is the fact that the second one only allows for the functionalisation of the outer layer of the biomorphs, which can be dissolved or washed by immersing the biomorph in a sodium hydroxide solution. The first method allows the functionalisation of the inner structure, resulting in a more robust functionalisation.

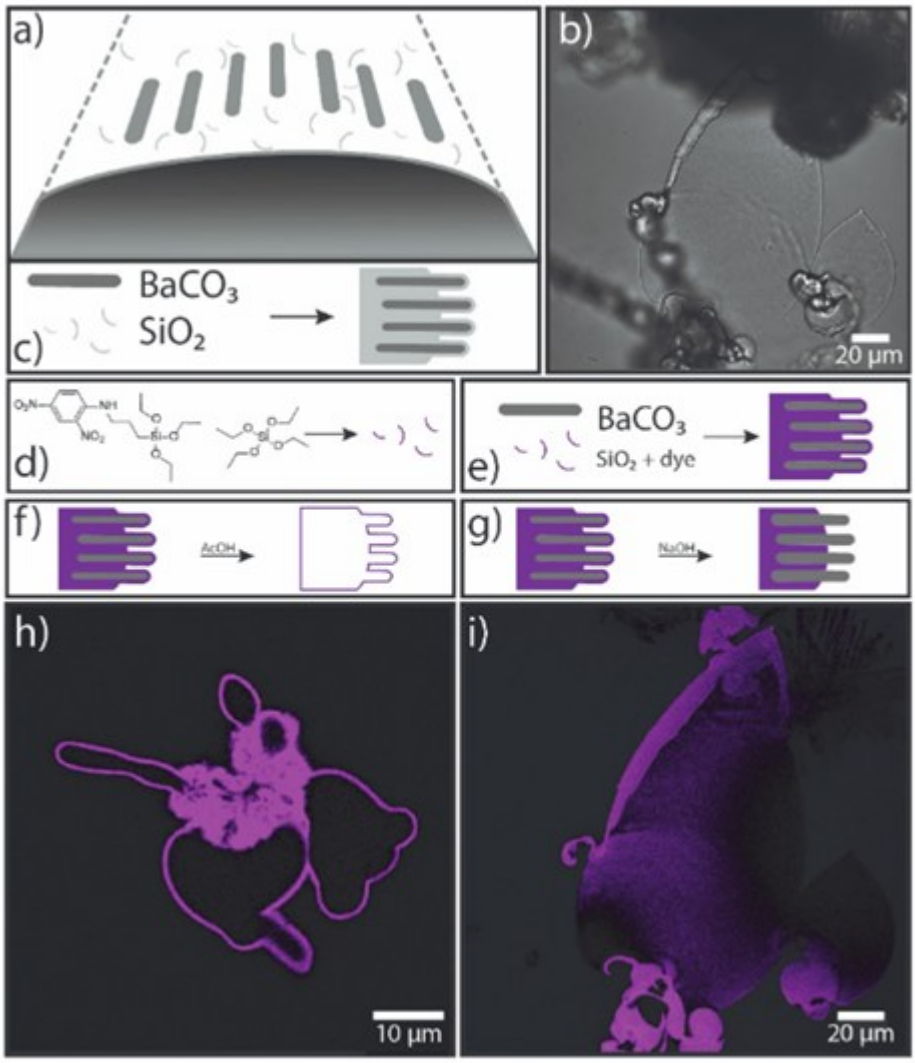

Figure 3 In situ functionalisation of biomorphs by silane co-condensation. (a) Schematic drawing of the growth of a biomorph by the continuous formation of carbonate nanocrystals (dark-grey rods) in the presence of silicate species (thin light-grey threads). (b) CLSM image (transmission channel) of a biomorph sheet. (c) Co-precipitation of $BaCO_3$ nanocrystals and unfunctionalised amorphous silica. (d) Co-condensation of TEOS and DNPTES into fluorescent "functional" silica. (e) Incorporation of fluorescently labeled silanes into the siliceous component of biomorphs (magenta-coloured domains). (f) Selective dissolution of the carbonate component by acid post-treatment, leading to a hollow silica structure. (g) Partial dissolution of the (outer) silica component by NaOH post-treatment. (h and i) CLSM images (fluorescence channel) of functional biomorphs after acid and base treatment, respectively. Reproduced from ref [6]

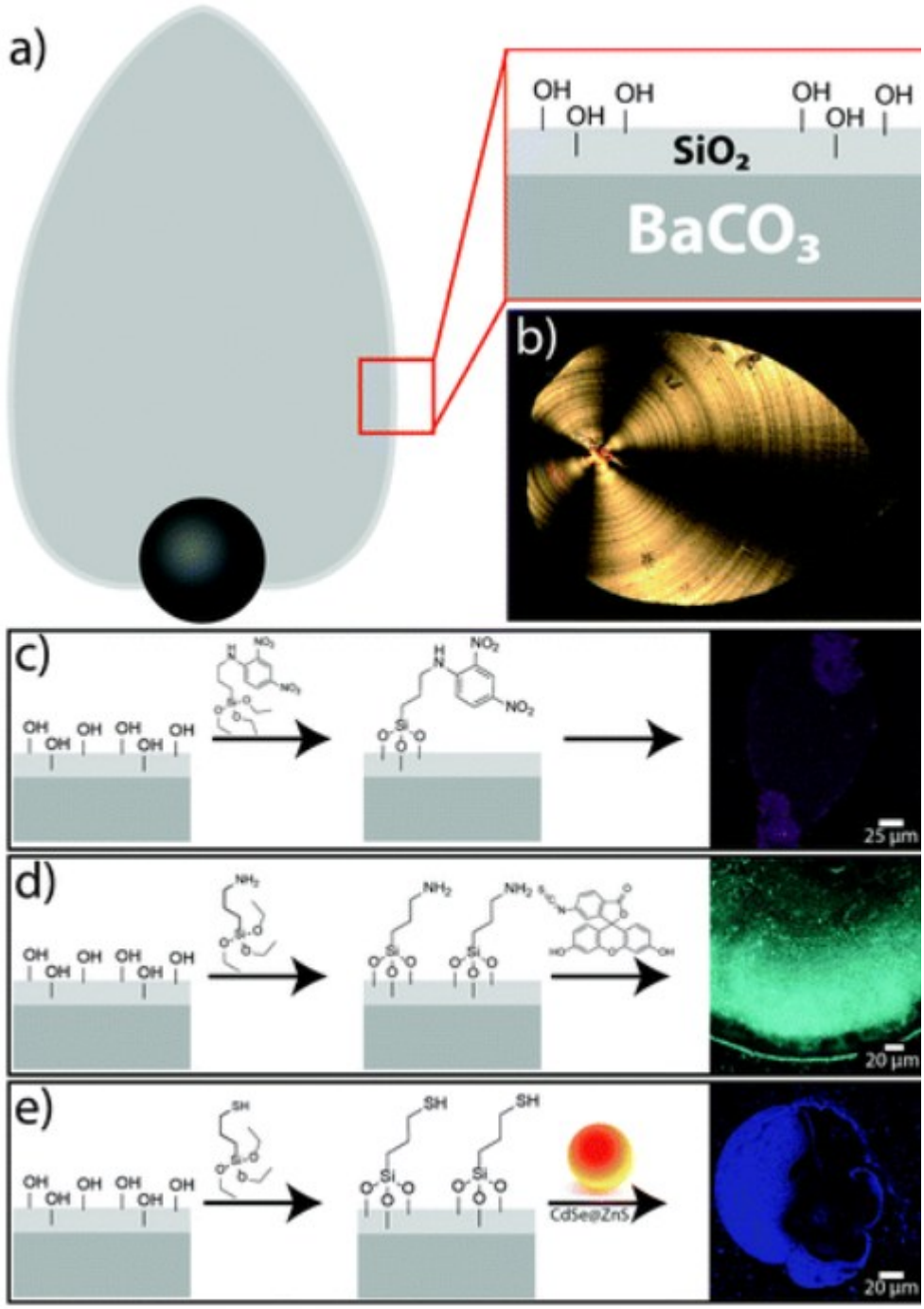

Figure 4 Post-functionalisation of biomorphs with different trialkoxysilanes. (a) Schematic drawing of a biomorph sheet with a thick outer silica skin carrying free silanol groups accessible for coupling reactions. (b) Polarised optical micrograph of a typical biomorph sheet. (c–e) Schemes for the post-silanisation of as-grown biomorphs with (c) DNPTES, (d) 3-APTES and further functionalisation with FITC, (e) 3-MPTES and subsequent binding of CdSe@ZnS quantum dots. In all cases, successful functionalisation is proven by corresponding CLSM images (right). Reproduced from Ref [6]

It has also been shown that it is possible to selectively dissolve the carbonate phase of the biomorph, leaving a hollow silica shell. This shell could then be used as template to precipitate other materials or be used as a capsule to carry specific contents. It also reinforces the potential role of the biomorphs in the early stages of life.

Biomorphs could have formed during a time where the conditions were more alkaline, then partially dissolve as the pH decreases, leaving hollow silica shell, potentially functionalised through the capture of simple organic molecules present in the medium. Those shells could provide a form of separation from the medium, thus playing the role of proto-cells.

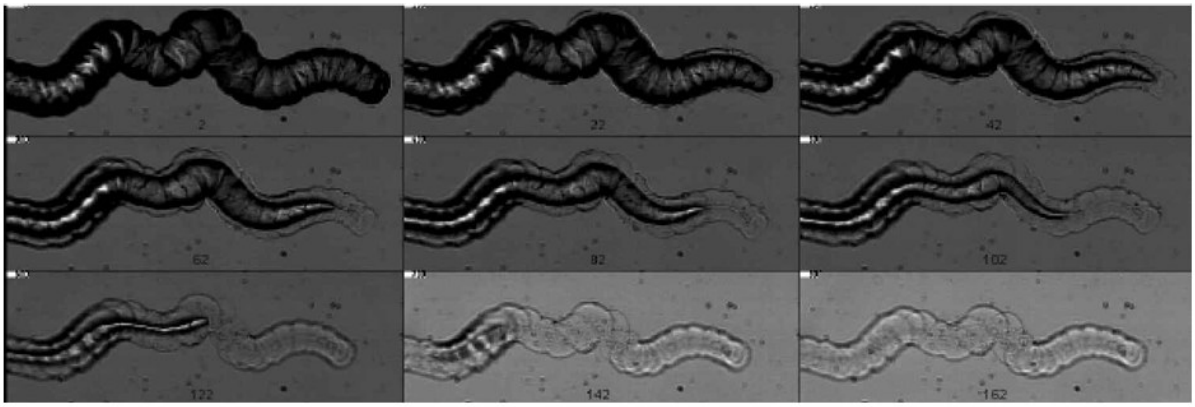

Figure 5 Time-lapse sequence (100 s between frames) showing dissolution of witherite crystallites within a bio- morph (on addition of 0.03 M acetic acid solution), from top left to bottom right. Note the conservation of the com- plex morphology in the silicate aggregate left (bottom right). Reproduced from Ref [7]

Apart from their potential biological role, biomorphs have been shown to be compatible with the subsequent crystallisation of other minerals, such as magnetite.[8] Inherently, biomorphs have no functionalisation, except for their unique shapes. We are then forced to modify them to give them desirable properties and open them to be used in nanotechnology. Opel J. *et all* were successful in forming biomorphs with a magnetite crystal formed on one end of the structure. They were able to show that the system was responsive to a magnetic field, allowing to move the magnetite-biomorph structure freely (figure 6). This opens the door to nanotechnology applications, allowing to exploit their unique shape while being crystalline materials.

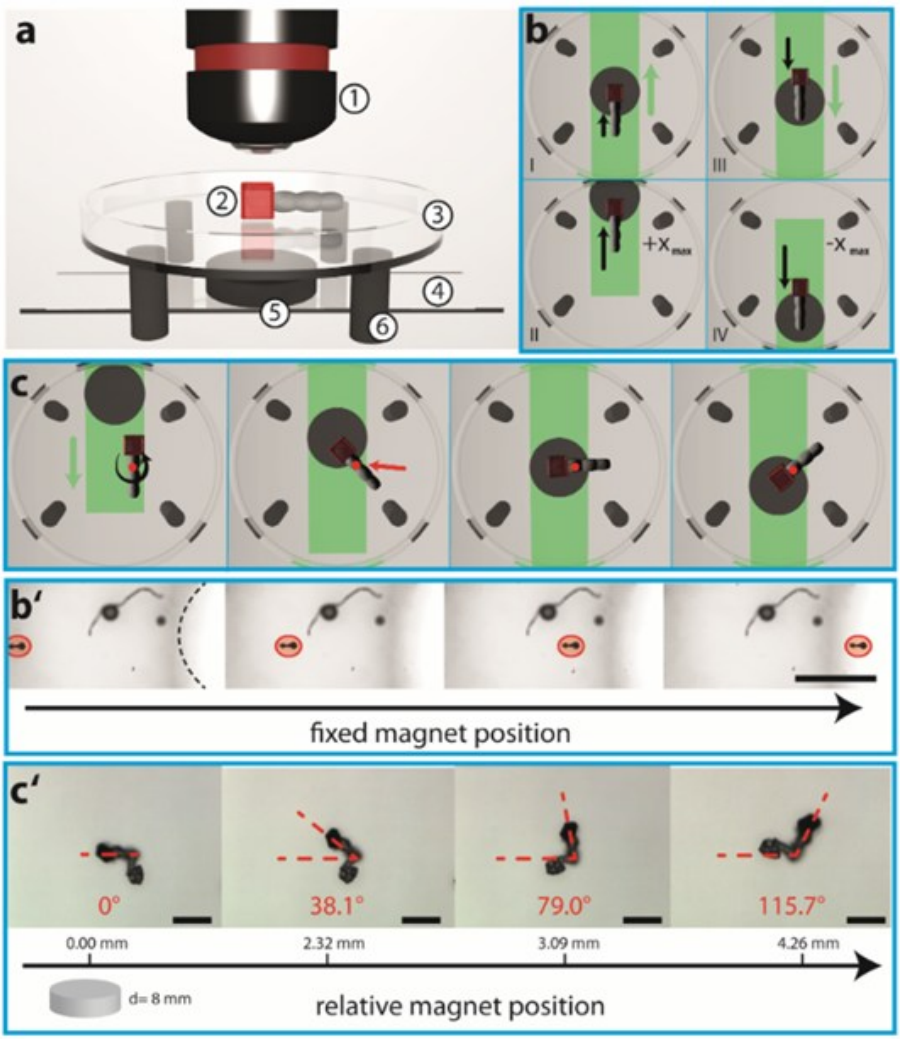

Figure 6 Biomorphs as responsive microarchitectures. a) Schematic illustration of the experimental setup used to move magnetized biomorphs in anexternal magnetic field—1: objective, 2: sample, 3: fixed Petri dish, 4: moving glass slide, 5: permanent magnet, and 6: holders for Petri dish. Movingthe object holder will only displace the magnet (and not the sample), whose relative position is tracked at all times. b) Sketch of a linear displacementof a magnetized biomorph across a highly viscous aqueous polyethylene glycol (PEG) solution guided by a permanent magnet. Green and black arrowsindicate the movement of the glass slide carrying the magnet below the Petri dish and the delayed response of the biomorph above, respectively. b') Snapshots of an experiment according to the setup in panel (b), where the magnet is located at the right end of the field of view as indicated by thedashed black line, while the magnetized microstructure (highlighted in red) is moving toward it. Scale bars are 1 mm. c) Sketch of a rotating movement (indicated by the black arrow) of a dry magnetized biomorph in response to a linear displacement of the permanent magnet (green arrow). The red dotmarks the position where the biomorph is fixed to the substrate (rotation axis), which in this case is not centered on the path travelled by the magnet.c') Snapshots of an experiment according to the setup in panel (c). The biomorph–mesocrystal composite responds to the movement of the magnet (relative positions are given below the microscopic images) by rotation as indicated by the drawn angles. Scale bars are 100 µm. Reproduced from Ref [8]

1.3 Formation mechanism

Biomorphs form when an alkali metal, specifically Barium, Strontium and Calcium, are put in basic (pH from 9 to 11) aqueous conditions in presence of silica and CO_2 (forming the CO_3^{2-} ions when dissolved in water). Additionally, biomorphs can be formed in two different systems: a silica and alkali metal solution in which atmospheric

CO_2 is let to diffuse or a silica gel (which can be doped with carbonate ions) in which the alkali metals diffuse. In both cases, the chemical species present in solution at those pH's are $Si(OH)_4$ in equilibrium with $SiO(OH)_3^-$ and $SiO_2(OH)_2^{2-}$ as well as HCO_3^- in equilibrium with CO_3^{2-}.

$$Si(OH)_4 \rightleftharpoons SiO(OH)_3^- + H^+ \rightleftharpoons SiO_2(OH)_2^{2-} + 2\,H^+$$

$$HCO_3^- \rightleftharpoons CO_3^{2-} + H^+$$

A study by *Menichetti et all*[9] of the pH and saturation index with Barium carbonate show the evolution of the saturation index and the pH at the diffusion front. They evidenced that the formation of the biomorphs occur at a narrow pH range of 10.3-10.4. In those conditions, the dominant silica species is $SiO(OH)_3^-$, which might indicate a possible significance of the role of silica in biomorphic growth. They also put in evidence the lack of biomorphs in the region near the interphase and explain it through the value of the pH being lowered by contact with the barium chloride solution.

The formation process is a sequential coprecipitation, triggered by the local variations in the pH as either the carbonate or the silica precipitate. As the carbonate precipitates, the CO_3^{2-} ions are used, displacing the equilibrium and producing more protons, thus locally acidifying the environment. This acidification causes the silica to precipitate, producing OH^- ions, locally increasing the pH of the environment, causing carbonate to precipitate again, and so forward.

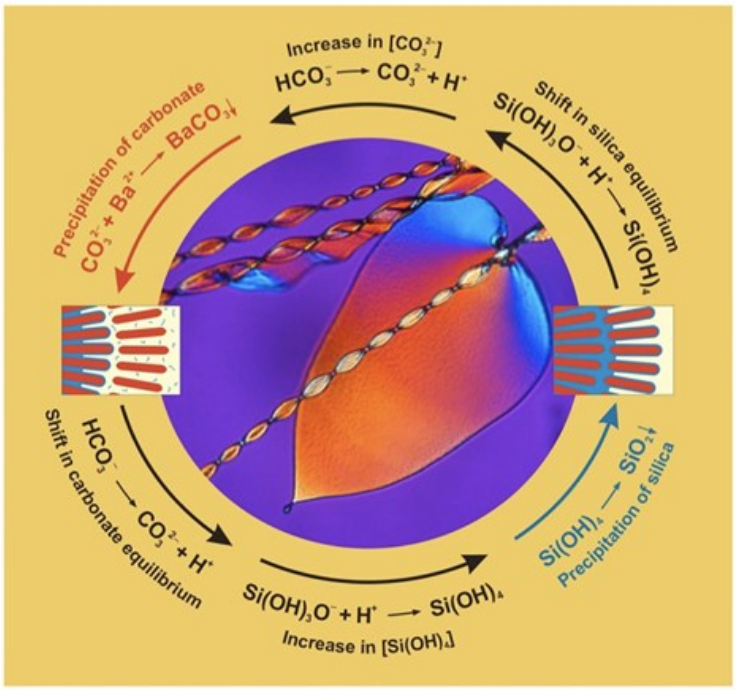

Figure 7 Cycle of silica-carbonate precipitation for the formation of biomorphs. Reproduced from [10]

2 Calcium carbonate

Calcium carbonate is an inorganic compound, widely present on Earth. It presents 3 polymorphs, as well as 2 hydrates. It can also precipitate as an amorphous material. Of the 3 polymorphs, calcite is the most stable under ambient conditions, followed by aragonite then vaterite. Both hydrated phases are unstable, and the transition towards the anhydrous calcite phases readily occur. The most common way to obtain monohydrocalcite is growing it in presence of magnesium ions, as they inhibit the formation of the anhydrous phases. The same can be done with phosphates in highly concentrated solutions to obtain ikaite, the hexahydrate of calcium carbonate. Additionally, ikaite can also be obtained using confinement in nano volumes. The amorphous phase is unstable and is thought to be mostly a transition state towards one of the anhydrous crystalline forms.

Table 1 Calcium carbonate polymorphs and hydrates.

Name	Composition	Symmetry	Space group
Calcite	$CaCO_3$	Trigonal	$R\bar{3}m$
Aragonite	$CaCO_3$	Orthorhombic	Pmcn
Vaterite	$CaCO_3$	Hexagonal	$P6_3/mmc$
Monohydrocalcite	$CaCO_3 \cdot H_2O$	Trigonal	$P3_121$
Ikaite	$CaCO_3 \cdot 6\ H_2O$	Monoclinic	C2/c

In solution, it has been shown that $CaCO_3$ often does not follow the classical crystallization theory and instead precipitates as a mixture of all 3 polymorphs, in addition to an amorphous phase.[11] The relative amount each of formed phases depends on both the pH of the solution and the saturation index (the logarithmic value of the supersaturation). The order of formation is generally as follows: first, the amorphous phase or a gel forms, followed by the formation of calcite and, in some cases, vaterite. Finally, after 24h, aragonite and vaterite (if not already present) are observed. Those crystals also exhibit various morphologies like calcite and aragonite spherulites or flower-like shapes for vaterite.

In nature, calcium carbonate is present in various rocks, such as chalk, limestone or marble, as calcite or aragonite. It has an important role in our industry as a primary component for construction or as additive in various other processes such as iron refining. Calcite and aragonite are the most common natural polymorphs, while vaterite is rarely found in nature. As both hydrates are unstable and tend to dehydrate, they are rarely found in nature.

Calcium carbonate is also used by living organisms as a structural material, like in the shells of marine molluscs and gastropods, eggshells or in pearls.[12-13-14] A protein framework is used to precipitate calcite and non-calcite crystalline forms, most commonly aragonite, but monohydrocalcite has also been observed. As calcite is the most stable form under ambient conditions, the formation of biological calcium

carbonate does not follow classical nucleation rules. The exact process is still not fully understood. The proteins not only influence the polymorphism but also the shape of the crystal structure.

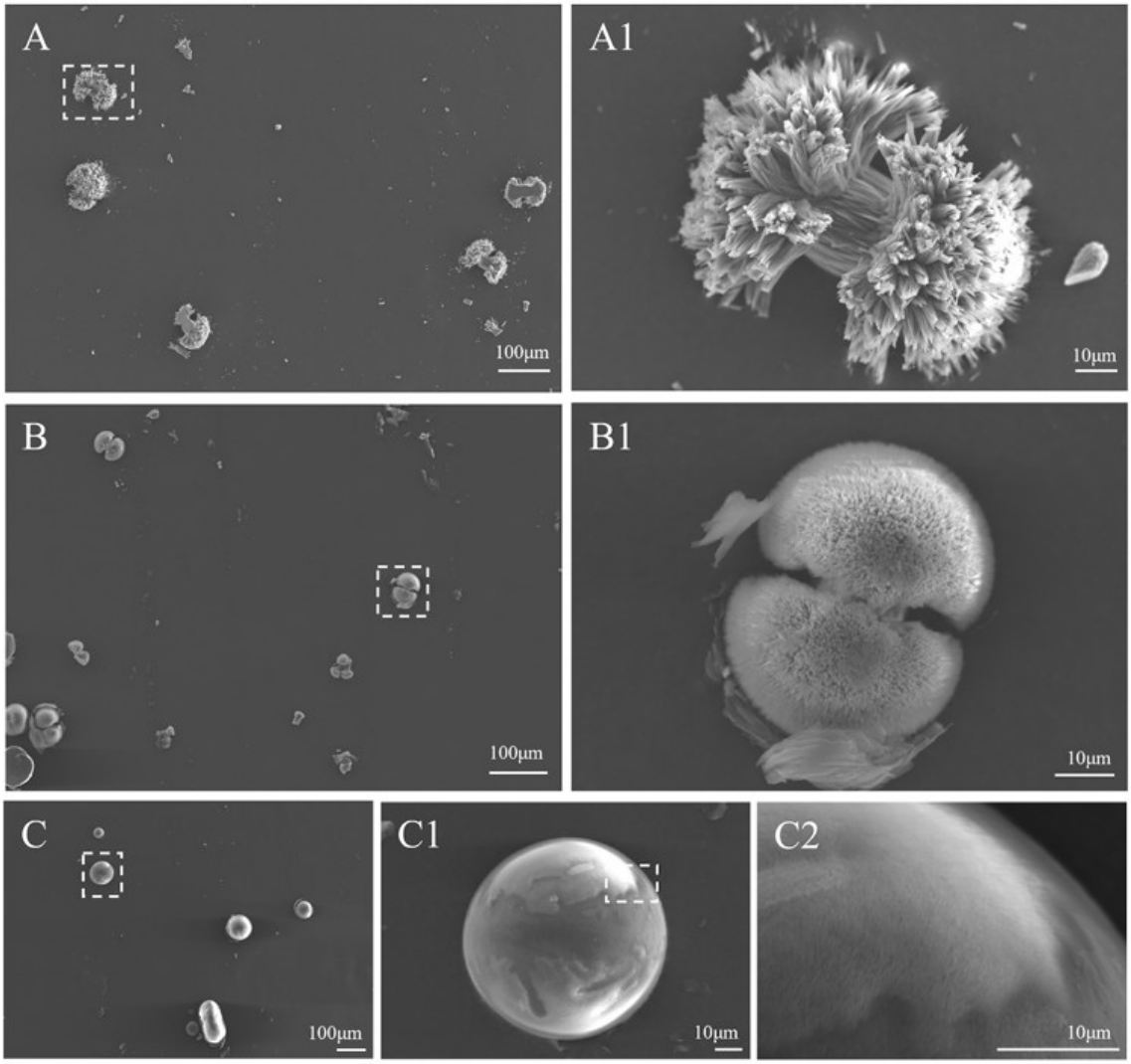

Figure 8 Effect of a recombinant protein on Calcium Carbonate precipitation. A & A1: Protein buffer, B & B1: Bovine serum albumin, C, C1 & C2: Protein Gh26. Reproduced from ref [12]

Monohydrocalcite has been studied by Ghan Zhang, for his PhD thesis with Professor Garcia-Ruiz, for it's potential to form biomorphs. In his work, he successfully obtained monohydrocalcite spherulites. This is realized without any additives, including magnesium, which otherwise is commonly used as it inhibits the growth of anhydrous calcite. Additionally, he was able to demonstrate a dependence on the temperature regarding the formation of biomorphic structures (figure 9). Using this, he was able to build multilayer biomorphs, with each layer grown at a different temperature, yielding complex biomorphic structures.[15]

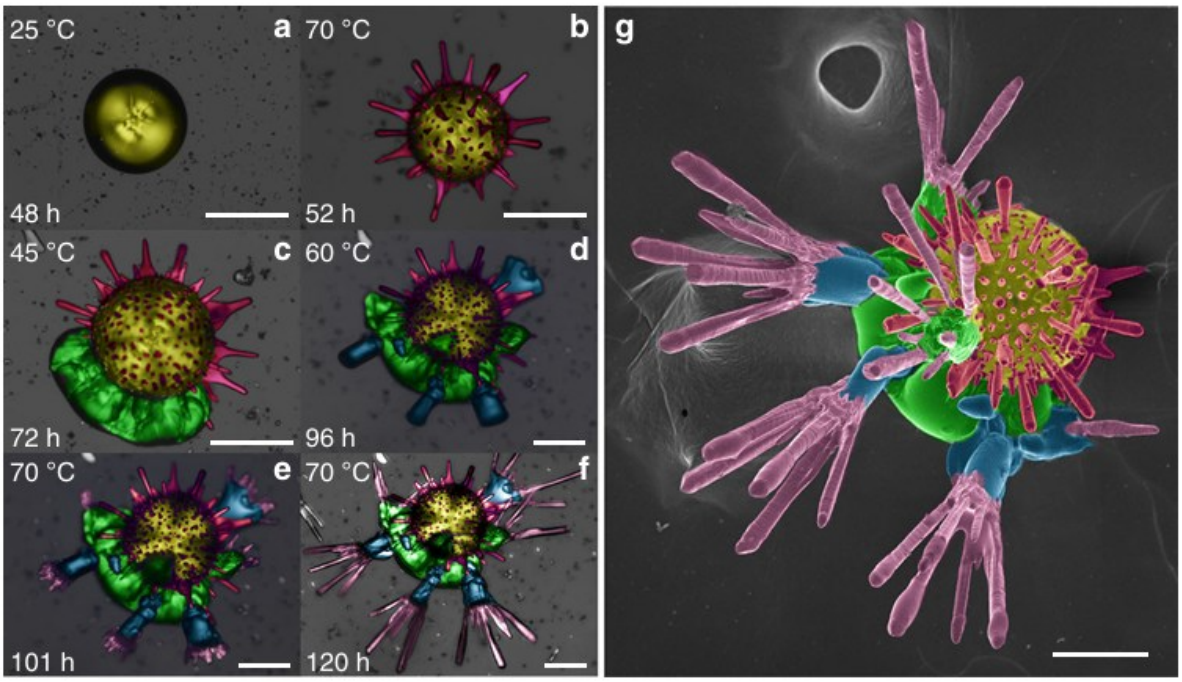

Figure 9 Growth history of multi-textured complex architectures of MHC. The growth periods at different temperatures have been labeled with false colors in both optical micrographs (a–f) and FESEM image (g): 48h growth at 25°C (yellow), 4h growth at 70°C (magenta), 20h growth at 45°C (green), 24h growth at 60°C (blue), 24h growth at 70°C again (purple), successively. The multi-textured MHC experience the growth at 25°C (0–48h), 70°C (48–52h), 45°C (52–72h), 60°C (72–96h), and again 70°C (96–120h). Scale bar: 100μm. Reproduced from ref [15]

During his work on monohydrocalcite, Ghan Zhan also reported the formation of aragonite, growing concomitantly in both time and space with calcite.[16] The aragonite presents the polycrystallinity and the smooth curvatures typical of biomorphs.

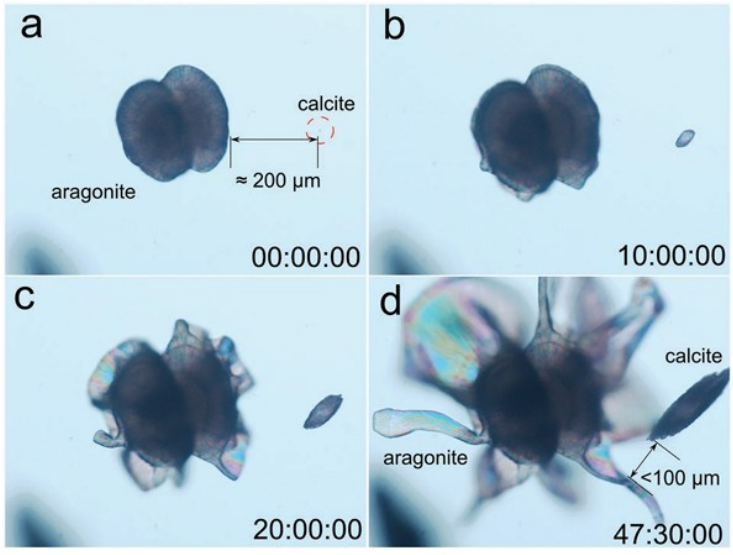

Figure 10 Selected frames of a time-lapse of the growth of an aragonite structure and a calcite crystal. It shows the proximity of the growing calcite crystal and the growing aragonite structure over time. Reproduced from ref [16]

3 Aim of the Thesis

The only work realised on biomorphic aragonite precipitation in silica gels is the discovery and report by Ghan Zhan. This work aims to describe the condition in which those biomorphs form and any morphological variations they might present.

The starting conditions of the experiment can be characterized by various factors. The starting pH of the gel is the first controllable variable, as it determines the amount of solubilized silica and its exact speciation. pH also influences the amount of carbonate ions dissolved in the gel liquid and its speciation. The pH also dictates the speed at which the silica gel forms. Restricting its values to above 10, gives enough time to manipulate the silica sol and ensure a homogeneous solidification.

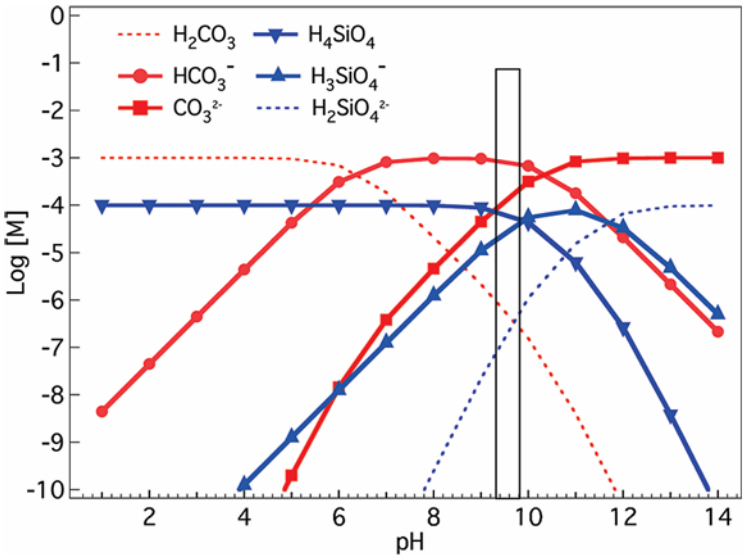

Figure 11 Logarithmic molar concentration of the ionic species of silica and carbonate against the pH. Produced based on the total amount of dissolved CO_2 and SiO_2 of 1 and 0.1 mM in water. Curves are plotted from equilibrium equation taking into account only the first two deprotonation of the acids. Reproduced from ref [17]

Another factor is the temperature at which the experiment takes place. As seen for monohydrocalcite, the temperature of crystallisation can lead to different morphologies. Furthermore, in the case of the crystallisation of calcite and aragonite, higher temperatures should favour the formation aragonite. To limit any potential effect from temperature, all experiments are realised at room temperature.

A factor that is not investigated here is the presence of additives or impurities, added with the objective of potentially modifying the crystallisation process. To study this type of effect, a good understanding of the pure system is needed first, which is the aim of this work.

The last parameter that can be modified is the initial concentration of calcium and carbonate introduced in the experiment. In order to study the effect of those variations on the formation of aragonite biomorphs, a morphogram of those structures is realised. This is done by screening the starting concentration from 0.1 mol/l to 1 mol/l of both calcium and carbonate, while keeping any other variable constant.

4 Experimental procedure.

The crystallisation experiments were conducted in a counter diffusion system, using homemade cassettes. Those are made of two glass plate, separated by a rubber and held with foldback paper clips. To ensure the proper sealing of the plates, the rubber band, vacuum grease is carefully smeared on it. To allow the injection of the solutions, 3 needles are placed, one on the side near the bottom, one on the side near the top and one on the top. Both side needles will be used to inject the solutions, while the top needle is there to allow the air to escape from the cassette. The internal dimensions are 9cm in hight, 3 cm in width and 1mm in thickness.

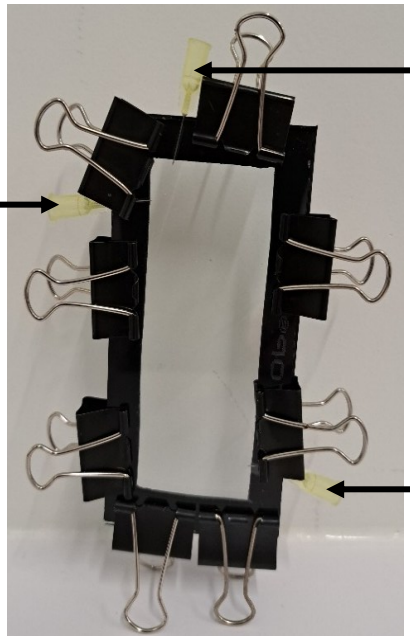

Figure 12 Empty glass cassette.

To prepare the silica gel, commercial silica solution (1.39 g/l, Sigma Aldrich) is diluted in a carbonate rich solution. The following equation is used to determine the volume used: $V_i = \frac{V_T(\rho_f - \rho_{H2O})}{(\rho_i - \rho_{H2O})}$ where V_i is the required volume of glass water, V_T is the final volume, ρ_{H2O} is the density of water (1 g/ml), ρ_f is the final density and ρ_i is the initial density (1,39 g/ml). The final density used for all experiments was 1.06g/l. To trigger the jellification of the silica, a fixed 3.5 ml of HCl 1 mol/l is added to 10ml of the diluted silica solution. This volume was determined in a previous work.

Both the sodium carbonate and the calcium chloride solutions were prepared by dissolving the solid in miliQ water. The mass used was calculated for each concentration.

To start the experiment, the cassette is filled with the acidified silica solution up to two third trough the bottom needle. The needle is removed once the liquid is injected. The cassette is then let 24h at ambient condition to allow for the jellification of the silica. The calcium chloride solution is then injected by the side top needle until the cassette is fully filled. Both the injection needle and the topmost needle are then removed. The diffusion and crystallisation will start immediately.

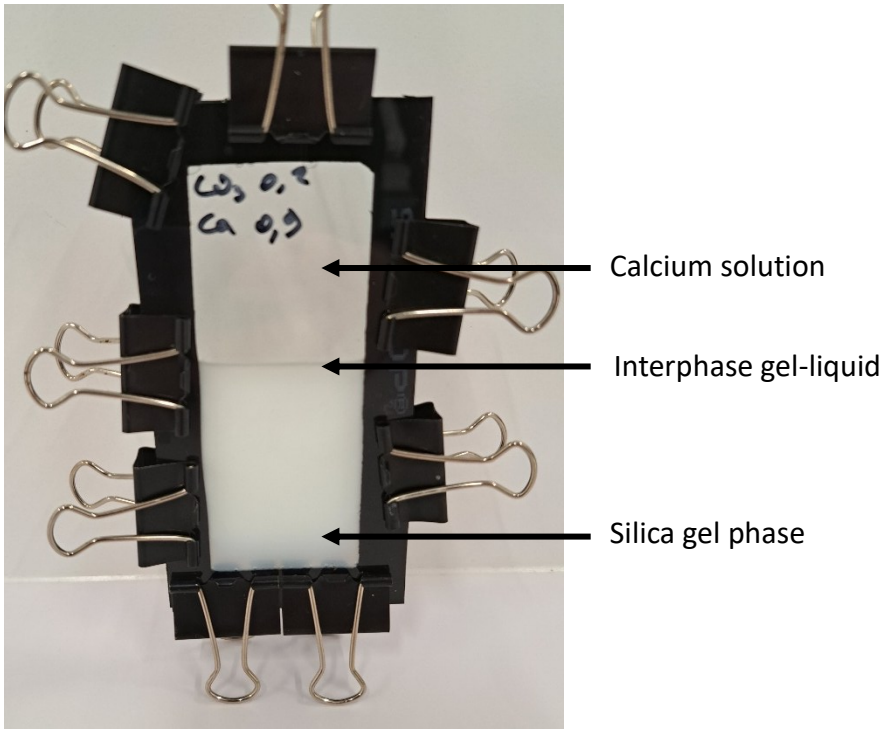

Figure 13 Filled cassette. The numbers are the concentration of calcium and carbonate ions. The cassettes are maintained in the pictured position during the diffusion.

The experiment is followed optical microscopy, with transmitted light. The microscopes used are a Nikon AZ100 microscope mounted with a CMEX-5 Pro USB camera and a Monopuit Anacrismat. The *in-situ* analysis of the crystals is realised by confocal Raman spectroscopy. The spectrometers used are a LabRAMHR spectrometer (Jobin-Yvon, Horiba, Tokyo, Japan) equipped with a laser diode emitting at a wavelength of 532 nm and a Thermofisher DXR coupled with a Continuum microscope, with a laser emitting at a wavelength of 532 nm.

5 Results

5.1 Raman spectroscopy

To identify the different polymorphs of calcium carbonate *in situ*, confocal Raman spectroscopy was used. As visible in Table 2, the main difference between the calcite and the aragonite Raman spectra is in the lattice mode, with aragonite presenting 2 close peaks at 152 cm^{-1} and 205 cm^{-1}, where calcite present two more distant peaks, at 154 cm^{-1} and 280 cm^{-1}. Another difference in those peaks is their sharpness, when observed in a silica gel matrix, calcite peaks are broader, and aragonite peaks are sharper. Another potential differentiation is the in-plane bending mode, as aragonite should present two close peaks (701 cm^{-1} and 705 cm^{-1}) and calcite only one peak (713 cm^{-1}). However, those two aragonites' peaks are too close to be distinguished and are visible as one peak.

Table 2 Raman wavenumbers of the calcium carbonate polymorphs

Form	Symmetric Stretching (cm^{-1})	In-plane bending (cm^{-1})	Lattice (cm^{-1})
Calcite	1084	713	154, 280
Aragonite	1084	701, 705	152, 205
Vaterite	1089	750	301

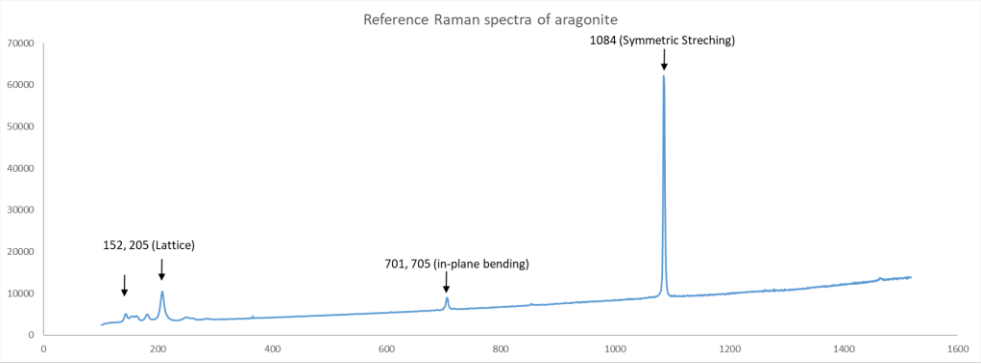

Figure 14 Reference Raman spectra of Aragonite. The different vibrations modes are highlighted. The in-plane bending shows as one peak. The lattice mode shows as 2 main peaks at 152 and 205 with smaller peaks in between. Data from ref [18]

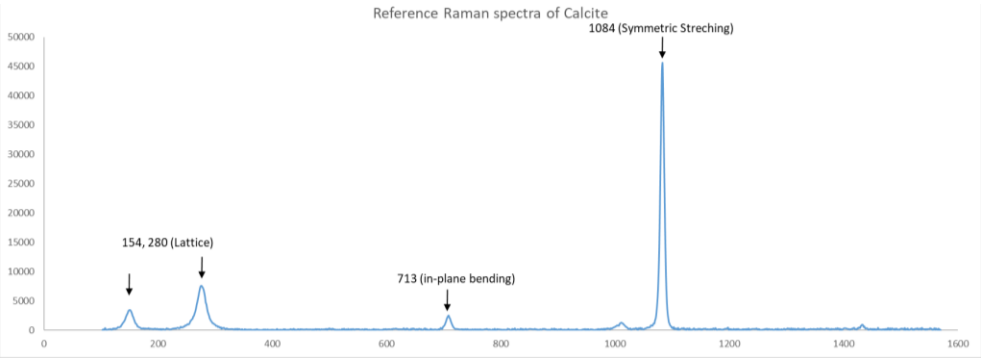

Figure 15 Reference Raman spectra of Calcite. The different vibrations modes are highlighted. The peaks at 1000 cm^{-1} and 1450 cm^{-1} are most likely impurities or artefacts. Data from Ref [19]

The insitu Raman spectra of the structures can then be compared to the references to determine if the analysed structure is composed of calcite or aragonite.

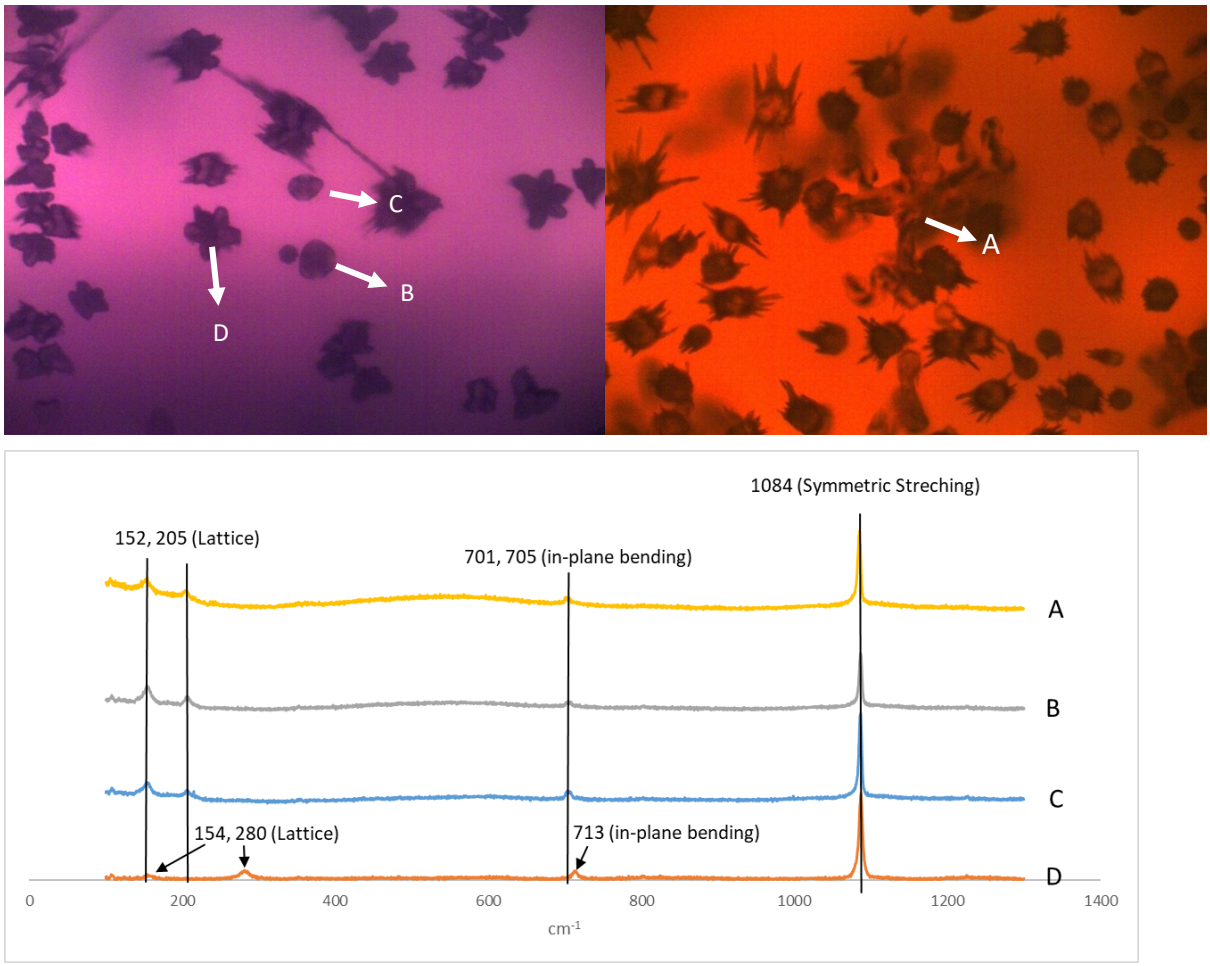

Figure 16 Raman spectra of calcium carbonate structures, each spectra correspond to the designated structures on the two top images. Experimental conditions: Left image: 0,5 mol/l of $CaCl_2$ & 0.2 mol/l of Na_2CO_3, Right image: 0,5 mol/l of $CaCl_2$ & 0.4 mol/l of Na_2CO_3. The different vibrations modes of each phase are highlighted, showing the differences for the in-plane bending and the lattice modes for calcite and aragonite. A, B and C correspond to aragonite, D correspond to calcite.

By analysing the Raman spectra of the 4 structures, it is visible that both structures A, B and C present the two peaks at 152 cm^{-1} and 205 cm^{-1} while the structure D present the two peaks at 154 cm^{-1} and 280 cm^{-1} (in this case, the peak at 154 is weak). Both the symmetric stretching and the in-plane bending peaks appear at their expected values but are too close to be of use when differentiating the phases, with the symmetric stretching of both calcite and aragonite being at the same position and the in-plane bending only varying of a few cm^{-1}. Using the lattice mode peaks, it can then be concluded that all 3 A, B and C structures are aragonite while the D structure is Calcite. The same process is applied to all experiments to identify the nature of the phase composing the structures. Through all the experiments, only calcite and aragonite were identified, no vaterite was observed.

5.2 Initial condition screening

The screening experiments can be represented in a table (Table 3). Each experiment was realised following the same procedure as described in the experimental part and the observation are done after one week (7 days) of diffusion. The conditions (concentration of calcium and carbonate ions) described for each experiment correspond to the initial conditions, not the conditions at the moment of observation. The cassettes are left at ambient conditions (20°C), in a room with minimal temperature change. While they were left upright for the time of the diffusion, they are laid down for observation.

As the objective is to observe the structures forming in the gel, it is important to determine the conditions allowing the homogeneous diffusion of the calcium in the silica gel. The screening reveals that the ratio Ca^{2+}/ CO_3^{2-} must be superior to 1 to allow for the diffusion to happen. In case where this ratio is lower than one, no diffusion is observed and only a few calcites crystals form in the first few millimetres of the gel (Figure 17). This lack of diffusion is due to the calcium precipitating at the liquid-gel interphase as it comes in contact with the carbonate-rich silica gel. The carbonate present deeper in the gel then diffuse toward the interphase, causing the calcite to precipitate continuously. Eventually, the carbonate will also diffuse in the liquid phase, causing the calcium to precipitate in the liquid phase, thus depleting it.

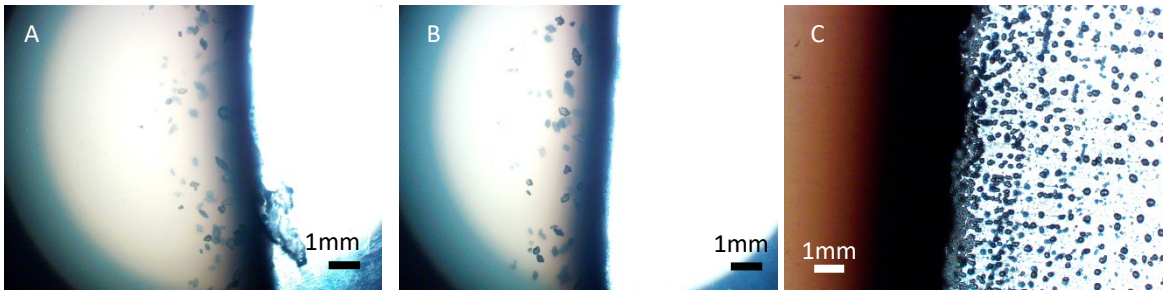

Figure 17 Optic image of the liquid-gel interphase for 3 different experiments with a Ca^{2+}/ CO_3^{2-} ratio inferior to 1. Experiment A and B show the formation of calcite crystals in the first 5mm of the gel from the interphase, with no further diffusion in the gel. Experiment C shows the formation of small crystals in the liquid phase, with no diffusion in the gel nor any crystals in the first 5 mm of the gel. Experimental conditions: A: 0,5 mol/l of $CaCl_2$ & 0.7 mol/l of Na_2CO_3, B: 0,5 mol/l of $CaCl_2$ & 0.6 mol/l of Na_2CO_3, C: 0,1 mol/l of $CaCl_2$ & 0.5 mol/l of Na_2CO_3

The screening results can be presented in a table. The grey part, with a Ca^{2+}/ CO_3^{2-} ratio lower than one, is of no interest for the rest of the study, as no diffusion happen. In green are all the experiments that lead to the formation of biomorphs. Not all combinations were made to save time. The orange experiments are those where diffusion did not happen even if a favourable ratio is given. This can be explained by the fact that the concentrations of both calcium and carbonate are high, causing a rapid precipitation at the interphase between the gel and the liquid. This would then lead to a blockage of the diffusion further into the gel. This is reinforced by the experiments in yellow, in which diffusion occurred but a noticeable line appeared, separating the gel into two parts. In the orange and yellow experiment categories, no aragonite is observed, only small calcite crystals and calcite crystal aggregates. In the case of the experiment with 0,1 mol/l of both $CaCl_2$ and Na_2CO_3, in orange as well, the lack of apparent diffusion can be attributed to the concentration being too low to lead to the formation of crystals in the gel.

Table 3 Representation of the diffusion behaviour of the experiments. Grey part represents the experiment with a Ca^{2+}/ CO_3^{2-} ratio lower than 1, leading to no diffusion. Green squares represent the experiment where a homogeneous diffusion is observed. Orange squares represent the experiments where no diffusion is observed despite a Ca^{2+}/ CO_3^{2-} ratio higher than 1. Yellow squares represent the experiments showing inhomogeneous diffusion.

Ca^{2+}(mol/l) / CO_3^{2-}(mol/l)	0.1	0.2	0.3	0.4	0.5	0.6	0.7	0.8	0.9	1
0.1										
0.2										
0.3										
0.4										
0.5										
0.6										
0.7										
0.8										
0.9										
1										

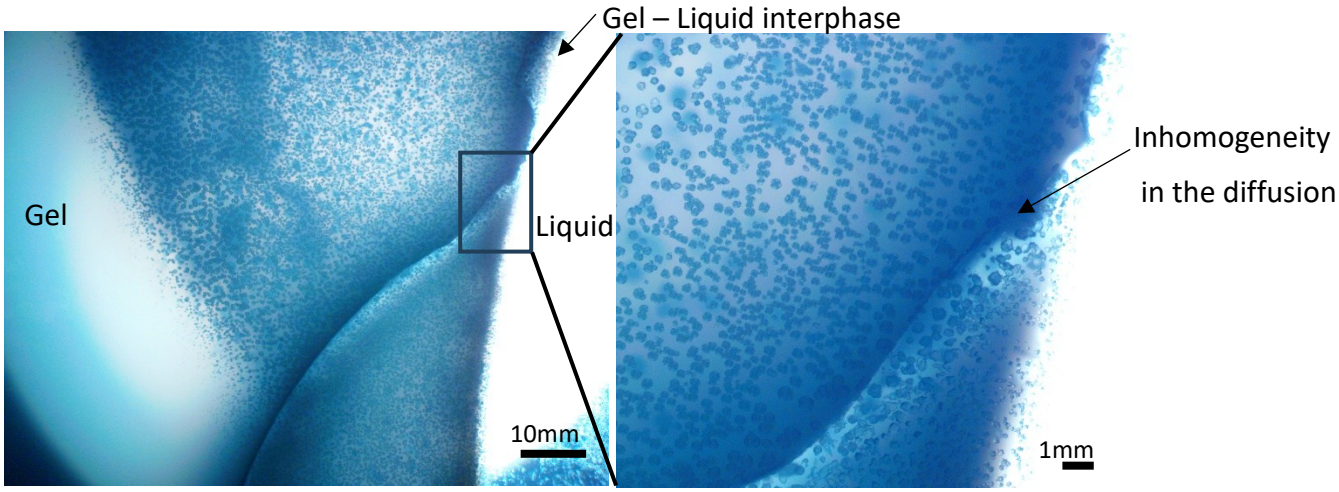

Figure 18 Optical microscopy image of the 0,8 mol/l of $CaCl_2$ & 0.7 mol/l of Na_2CO_3 experiment after 1 week. Pictured is an inhomogeneity in the diffusion, with a clear separation of the diffusion zone in the gel in two parts. This inhomogeneity might be caused by the high overall concentration of both carbonate and calcium ions, causing a high precipitation rate and leading to a blockage of the diffusion.

A global effect of the concentration of calcium and carbonate ions is the distance the calcium diffuses in the gel. This distance is dependent on the concentration of the starting solutions, but is usually between 3 to 5 cm, with it going further the higher the initial concentration of calcite, except for the cases mentioned earlier, such as the absence of diffusion or the presence of an inhomogeneity in the diffusion.

An analysis of the both the calcite structures and the aragonite structures in the experiments highlighted in green will help identify any pattern or evolution depending on

either the Ca^{2+}/ CO_3^{2-} ratio or the overall concentration of both ions. By studying the morphological trends of both type of structures, then studying the formation conditions of the calcite structures, which have been more widely studied, we can estimate the condition present at each point in the gel. This will allow us to determine the formation condition of the aragonite structures.

5.2.1 Calcite structures

The calcite structures present a constant pattern across all experiments. Starting with small crystals following the classic trigonal geometry of calcite in the first few millimetres in the gel. Quickly, the calcite starts showing deformations, appearing first as aggregate with the silica blocking the growth of some of the faces. This is followed by single crystallites showing a typical deformation caused by silica, where it's faces are blocked, only allowing the edges to grow, forming what looks like long spikes. These structures are present either as a single crystal or as an aggregate of crystals, with the edges all growing following the same axis. The calcite then changes again and starts forming bi-cones structures, linked by their summit. In the end part of the diffusion, the calcite structure takes the form of spheres with spikes shooting out, resembling stars. This pattern is present in all experiments where diffusion took place. The main variation is the exact size of the area where each type of structure appears. As mentioned, the higher the initial calcium concentration, the further in the gel the diffusion goes, thus leading to bigger area for each type of structures.

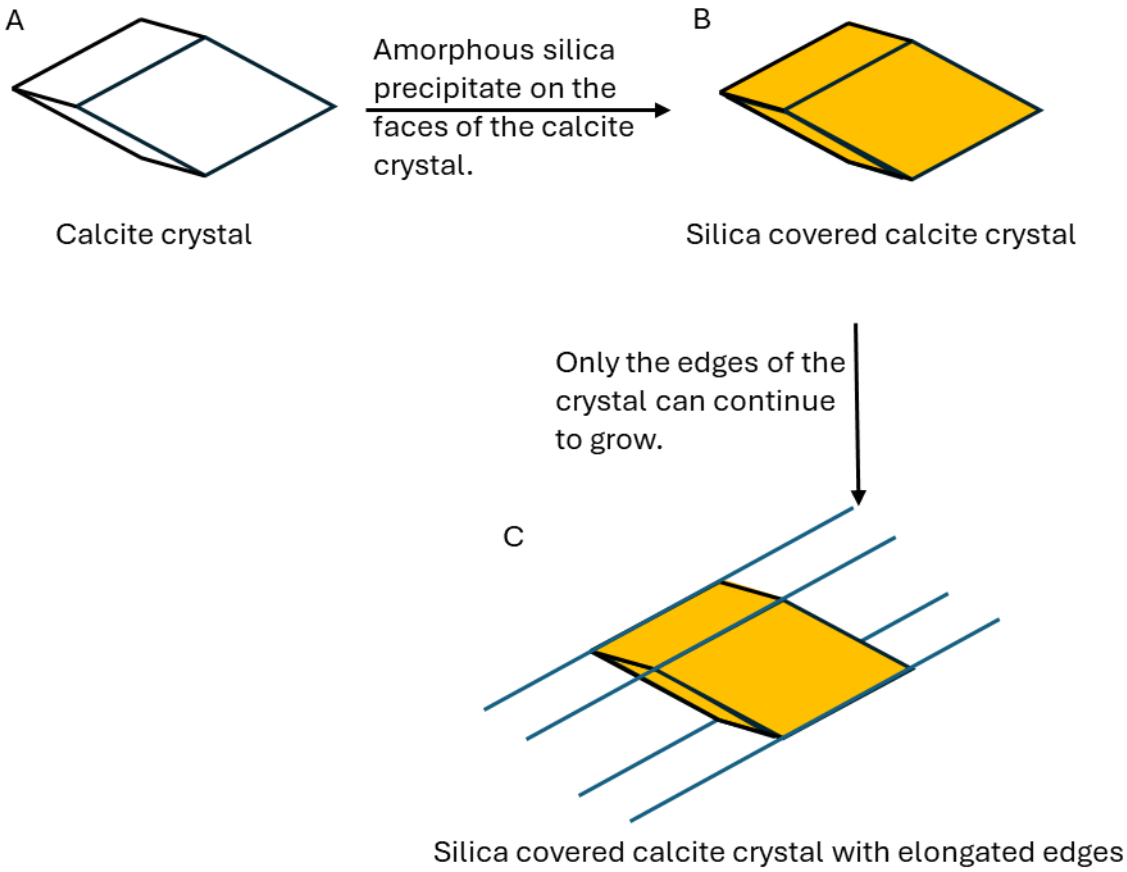

Figure 19 Schematic representation of the formation of the deformed calcite crystals with elongated edges. A: a normal calcite crystal forms. The formation of the crystal causes the acidification of the local environment, leading to the precipitation of amorphous silica. B: The faces of the calcite crystal are covered in amorphous silica, impeding the growth of the crystal. C: As only the edges of the crystal are allowed to grow, a rod like calcite formation extrude from the crystal, forming the structure with elongated edges.

Table 4 Selected examples of the evolution in space of calcite structures. First row (image A, F and I) show the structure at the interphase mostly classical calcite crystals. Second row (images B, G and K) show the structures appearing between 5 to 10 mm in the gel from the interphase, deformed calcite crystals forming aggregates. Third row (images C, H and L) show the structures appearing between 10 to 15 mm in the gel from the interphase, deformed calcite crystals, with elongated edges. Last two row (images D, E, I, M and N) shows the structures appearing past 15 mm and until the end of the diffusion, bi-conal and star-like calcite structures. All images are taken after 7 days of diffusion. Scale: A to I: 500µm, J to N: 100µm.

Type of structures	0,5 mol/l of $CaCl_2$ & 0.4 mol/l of Na_2CO_3	0,8 mol/l of $CaCl_2$ & 0.5 mol/l of Na_2CO_3	0,7 mol/l of $CaCl_2$ & 0.2 mol/l of Na_2CO_3
Interphase: Regular calcite	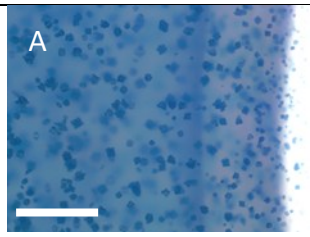	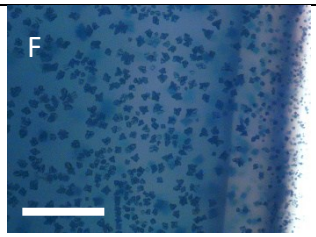	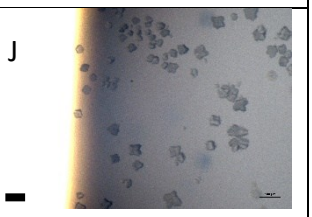
5 to 10 mm in the gel: Deformed aggregate	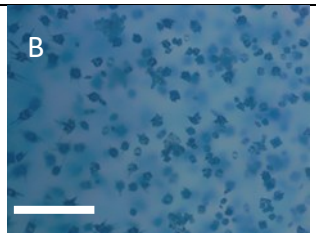	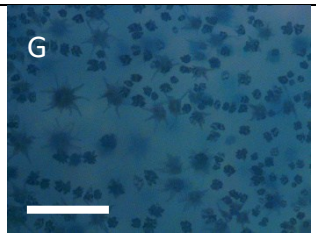	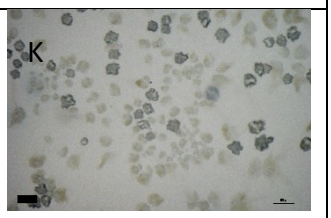
10 to 15 mm in the gel: Edge elongated crystals	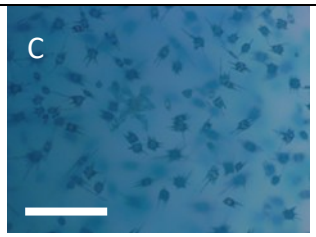		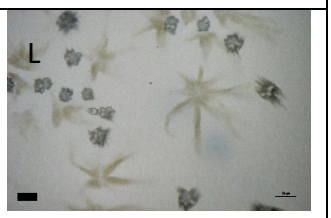
15 to end of diffusion (30~40 mm): Stars and double cones		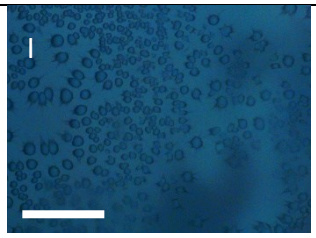	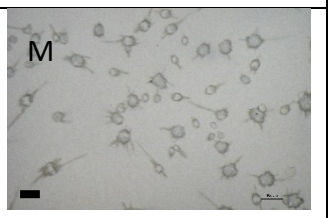
	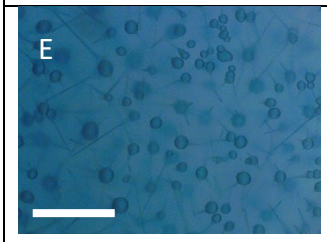		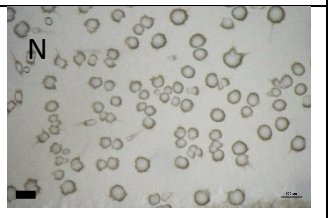

5.2.2 Aragonite structures

The aragonite structures never appeared in the first few millimetres of the gel and stop forming after 10 to 15 millimetres in the gel, creating a restricted zone in which aragonite structures appear next to and at the same time as the calcite structures. The reason of this absence could be the same as the reason for the lack barium biomorphs in the interphase between the gel and the liquid.[9] In that region, the pH is strongly influenced by the alkali metal solution, leading to a sharp decrease. This leads to the aragonite structure always appearing together with the deformed calcite crystals.

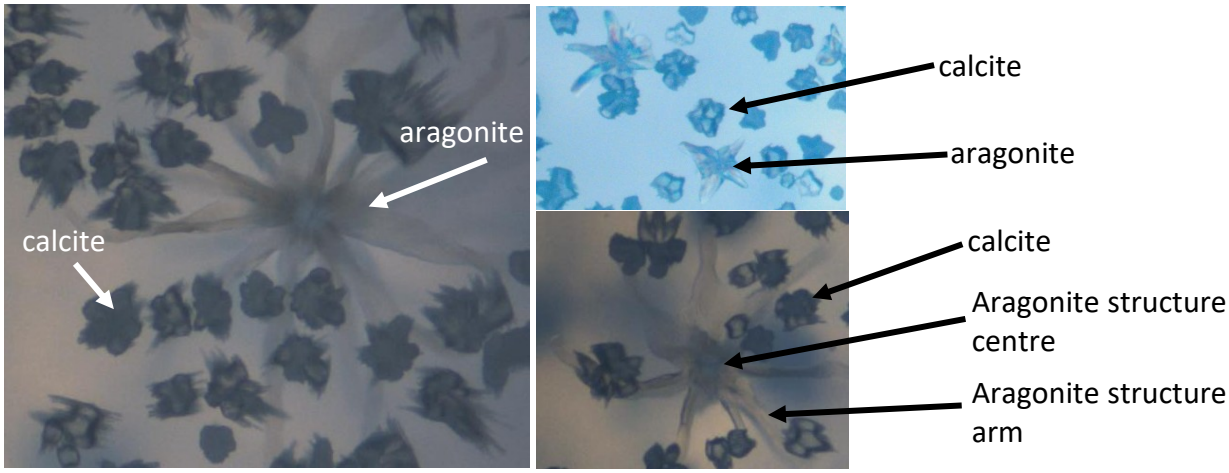

Figure 20 Selected examples of aragonite structures. Aragonite forms star-like shapes, with arm expanding from the centre of the structure. Calcite is present as deformed crystal and crystal aggregate.

Firstly, we can look at the evolution of the calcite structures depending on the concentration of carbonate, while keeping the concentration of calcium constant at 0.5mol/l.

The structures of interest in Figure 21 A and B are the small spheres, which were confirmed to be aragonite by Raman spectroscopy. The main evolution with the concentration of carbonate is the size of the structure. In figure 7 C and D, the aragonite structure grows bigger, from ~150µm to 300µm. The morphology changes as well, the structures are made of arms expanding from a centre, curving smoothly and rapidly into spirals. In Figure 21 E, we observe another change in morphology, with a structure made of arms expanding out from a centre, showing once again smooth curvatures but further away from the centre. The curvature is also not as pronounced as in the two previous images (Figure 21 C and D), not forming spirals but long curves, with the arms expanding several hundred of micrometres in the gel. This series of experiment allow us to distinguish 3 types of morphology: the spheres, the short and rapidly twisting structures and the longer and bigger structures, with gentler curvatures. This series also reveal an increase in size of the structures with the increase in concentration of carbonate.

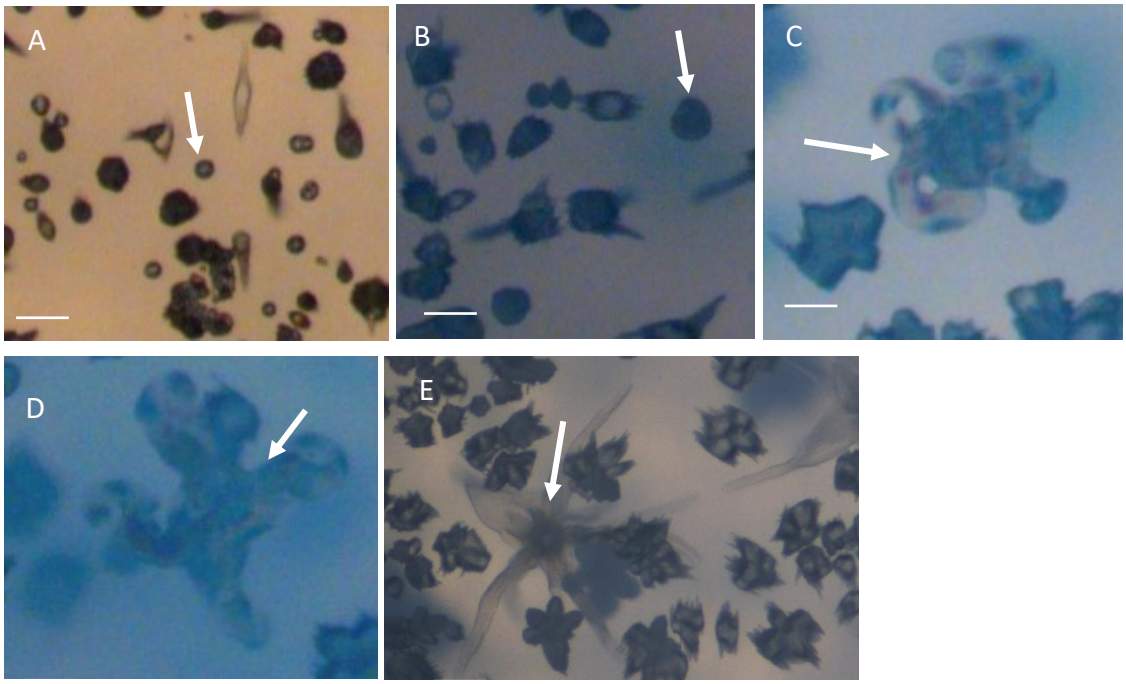

Figure 21 Optic microscopy image of: A: 0,5 mol/l of $CaCl_2$ & 0.1 mol/l of Na_2CO_3, B: 0,5 mol/l of $CaCl_2$ & 0.2 mol/l of Na_2CO_3, C: 0,5 mol/l of $CaCl_2$ & 0.3 mol/l of Na_2CO_3, D: 0,5 mol/l of $CaCl_2$ & 0.4 mol/l of Na_2CO_3, E: 0,5 mol/l of $CaCl_2$ & 0.5 mol/l of Na_2CO_3. Scale bare is 50 µm. Aragonite structure are marked by an arrow. Image A and B show small spherical aragonite structures. Image C and D show bigger structures, with arm rapidly curving on themselves. Image E show a bigger structure, with arms expanding from a centre point and curving smoothly and gently.

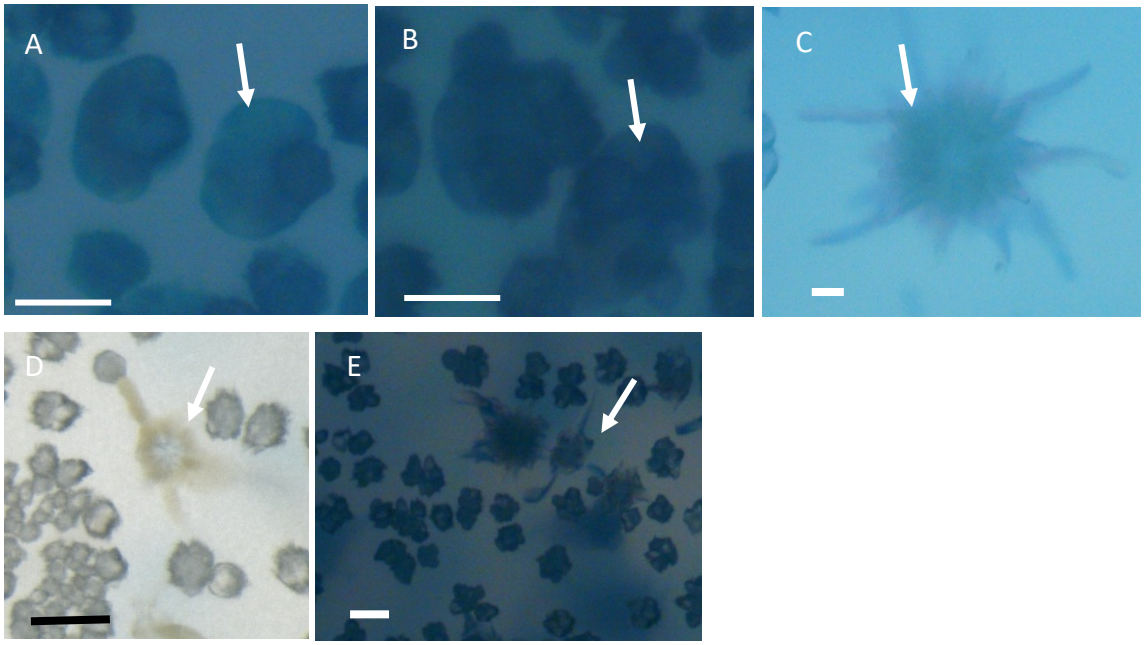

Figure 22 Optical microscopy images of: A: 0,6 mol/l of $CaCl_2$ & 0.5 mol/l of Na_2CO_3, B: 0,7 mol/l of $CaCl_2$ & 0.5 mol/l of Na_2CO_3, C: 0,8 mol/l of $CaCl_2$ & 0.5 mol/l of Na_2CO_3, D: 0,9 mol/l of $CaCl_2$ & 0.5 mol/l of Na_2CO_3, E: 1 mol/l of $CaCl_2$ & 0.5 mol/l of Na_2CO_3. Scale bare: A, B, C: 50 µm, D and E: 100 µm. Aragonite structures are marked with an arrow. Image A and B show a spherical structure. Image C and D show an aragonite structure with short arms, curving rapidly (they curve out of the focal plane in the case of image D). Image E show an aragonite structure with expanding arms.

The same series of experiment is done for the calcium concentration, keeping the carbonate concentration constant at 0.5 mol/l and varying the calcium concentration from 0.5 to 1 mol/l (Figure 22).

We can once again look at the evolution of the morphology of the aragonite structures. In Figure 22 A and B, the aragonite is present as spheres. While similar to the structures in Figure 21 A and B, they are bigger and are not perfectly spherical. In Figure 22 C and D, the aragonite forms structures with short, curving arms, rapidly exiting the depth of field of the microscope. In Figure 22 E, the aragonite forms bigger structures, with arms expanding further before curving. As for the increase in concentration of carbonate, we observe an increase in size with the increase in calcium concentration.

Based on the previous two experiment series, we can then create 3 categories of aragonite structures: sphere (like in Figure 21 A and B and Figure 22 A and B), highly twisting structures (like in Figure 21 C and D and Figure 22 C and D) and large expanding structures (like in Figure 21 E and Figure 22 E). They can be added to the table to give the morphogram in Table 6. This table reveals a tendency to form structures with elongated arms at higher concentrations of calcium (above 0.6 mol/l) while lower concentrations favour the formation of the smaller twisting structures. The formation of the aragonite sphere does not seem to follow a pattern but could be linked to the speed of precipitation of the calcium carbonate. In all of the experiments forming spheres, a high density of crystals was observed as well. Those spheres could then be the result of an early interruption on the grow of the biomorph, and, if this high density of crystallisation did not occur, could have led to the formation of either type of biomorph. This table also highlights the fact that the diffusion seems not to occur properly at carbonate concentrations higher than 0.5 mol/l, leading to either no diffusion in the gel or the formation of breaking lines in the gel and an inhomogeneous diffusion. It also appears that verry low concentrations of both calcium and carbonate will lead to no apparent diffusion.

Table 5 Morphogram of aragonite structures. Orange: Blocking ate the interphase; Yellow: divition of the diffusion; Purple: Aragonite spheres; Pale green: Aragonite twisting structures; Bleu: Aragonite long expanding structures.

CO_3^{2-}(mol/l) \ Ca^{2+}(mol/l)	0.1	0.2	0.3	0.4	0.5	0.6	0.7	0.8	0.9	1
0.1										
0.2										
0.3										
0.4										
0.5										
0.6										
0.7										
0.8										
0.9										
1										

5.3 Electron Scanning microscopy

Some selected structures were also observed with scanning electron microscopy. The selection method was purely visual and only experiments with larger and well-defined structures were chosen. To be able to observe them by SEM, the structures were taken out of the plate, by opening it and "fishing" the crystals with a set of micro-tools. They were then washed with water and a solution of NaOH 1mol/l, to remove as much silica gel as possible. The crystals were then placed on carbon tape mounted on the sample holder. A step of metallisation is then performed with carbon.

By using a broken off arm of an aragonite biomorph, it is possible to reveal the internal structure. The arms of the biomorph are seemingly composed of sheets, stacked radially. The twists can then be explained by a difference in growth of those sheets: if they are thinner or shorter on one side, the structure will start curving toward that side. The surface of the biomorph is still covered in residual silica gel, forming small spheres.

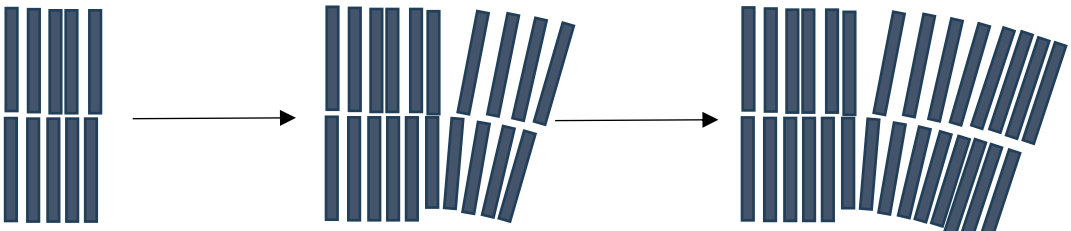

Figure 23 Schematic representation of the curving in an aragonite biomorph. As the tip of the biomorphic aragonite arm grow, a difference is the size of the aragonite sheets causes the arm to curve towards the side with the shortest sheets. Once the sheets are growing to the same size on both sides, the arm grow straight again.

There was no access to the centre of the structures, as non were broken, thus it is not possible to say if the internal structure of the arms and the centre are the same.

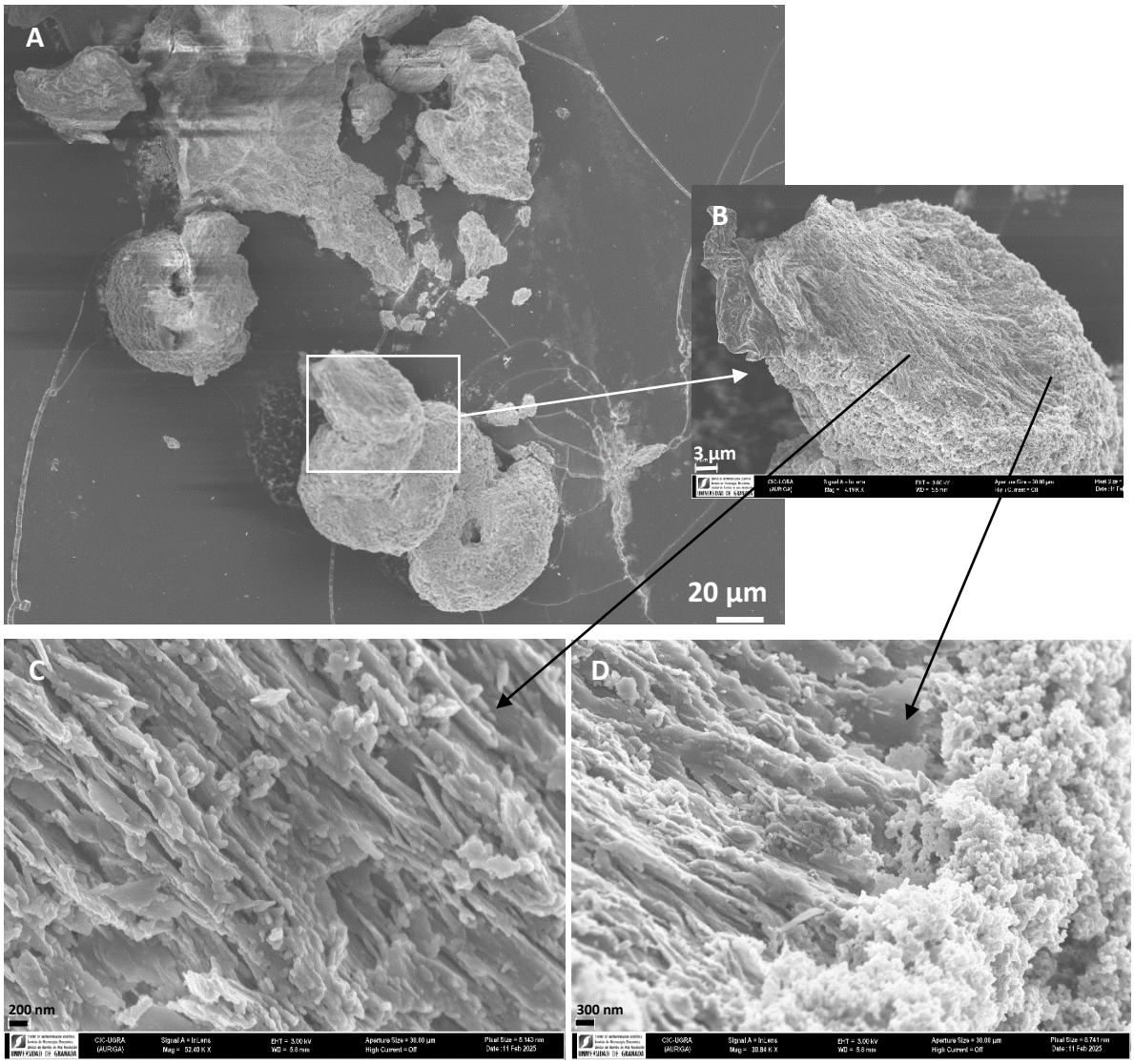

Figure 24 SEM image of a broken off arm of an aragonite biomorph. The sheet-like structuration is visible on the magnified images (C and D)

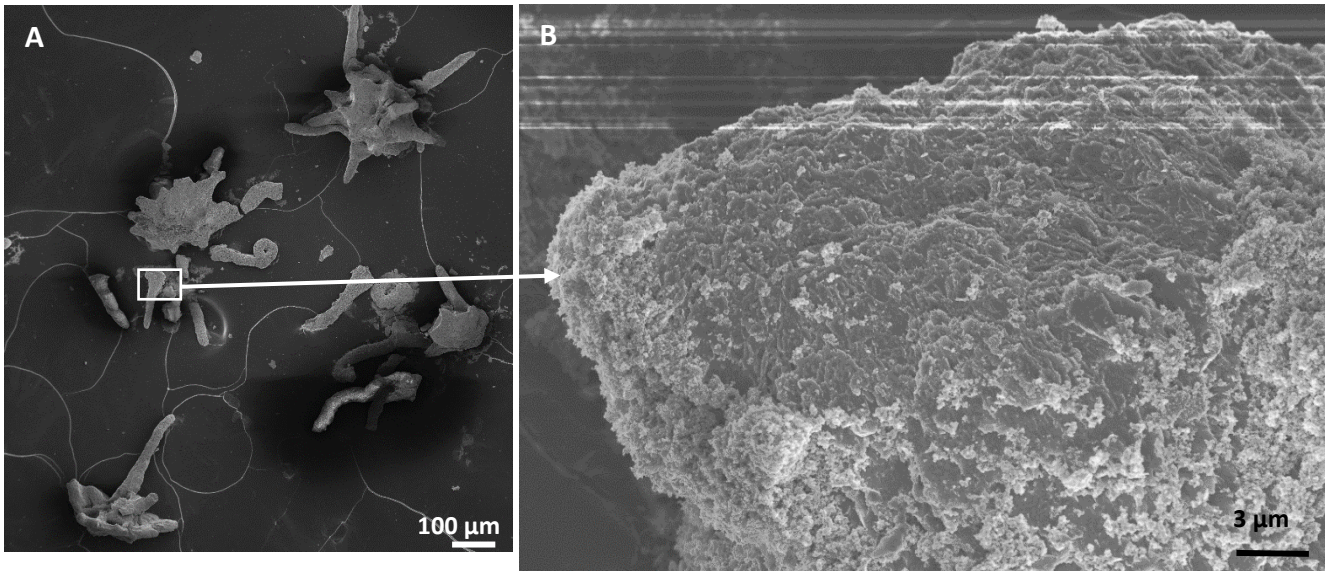

Figure 25 SEM image of a broken off arm of an aragonite biomorph. The sheet-like structuration of the aragonite is visible in the magnified image (B).

Aragonite structure can also be compared to the calcite structures. The selected structures are the ones that form further in the gel, such as the diabolo-like structures or the star-like structures, as they are polycrystalline and present unique shapes, where the original calcite structure is no longer visible.

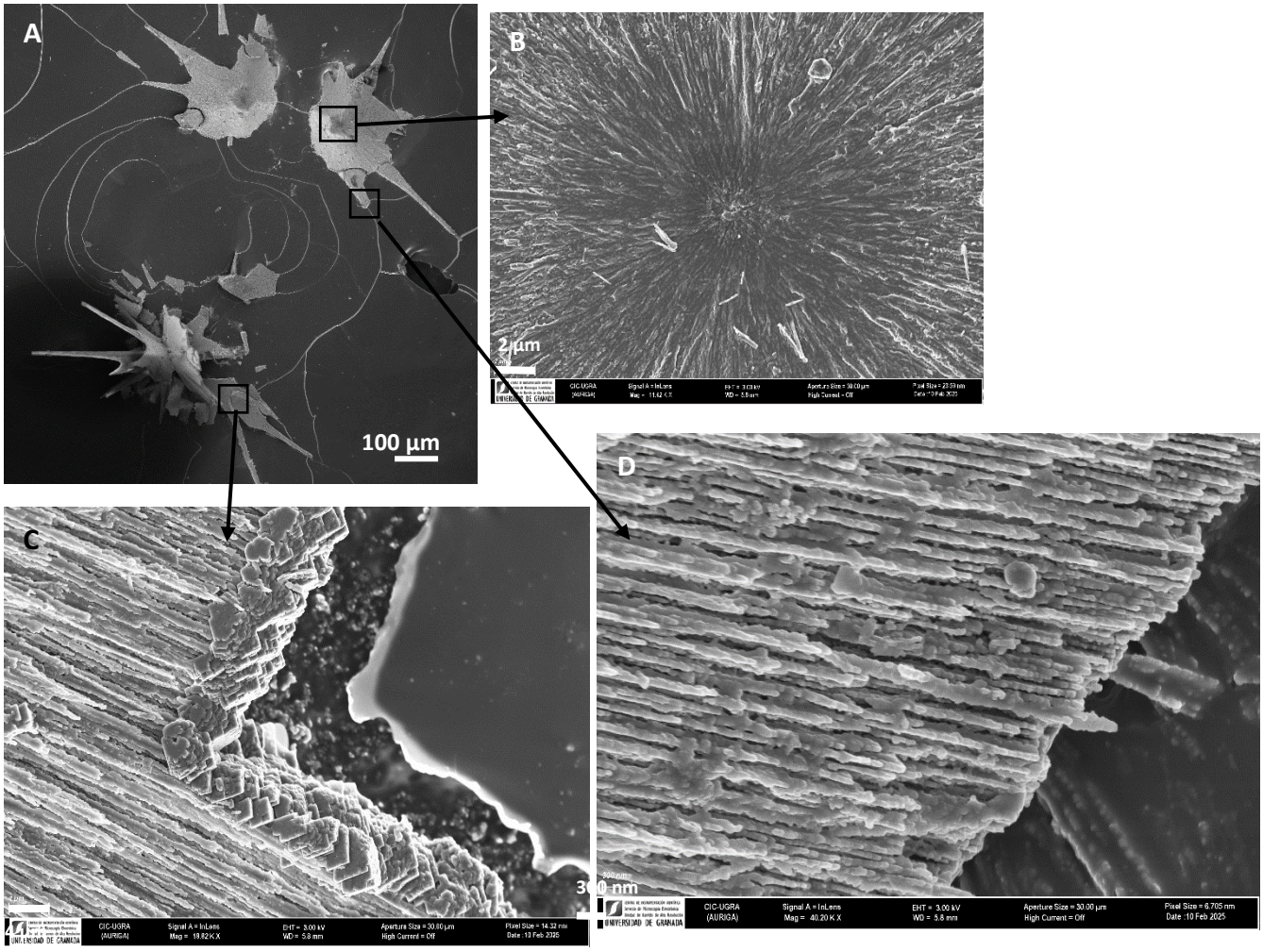

Figure 26 SEM image of a calcite diabolo-like structure. The magnified image D allow to see the rod-like structuration of the calcite. The magnified image of the rupture point C allows to see the trigonal crystalline geometry of the calcite.

Diabolo-like calcite structures are composed of rods, aligned and stacked, forming sheet-like structures. All rods are aligned towards the edge of the sheet. Breaking points in the structure show a retention of the trigonal crystal structure. At the centre of the structure, were the two cone forming the diabolo meet, the rods start in the centre and extend toward the exterior. The surface also shows a lower retention of the silica gel compared to the aragonite structure, having followed the same treatment. This rod structure is also found in the calcite stars, forming the spikes going out of the centre.

For calcite stars, the centre was not accessible, but the spikes clearly show the rod structure, oriented in the axe of the spike. Broken off sections allow to study the interior of the spike, where the trigonal geometry of calcite is found. The star seems to have retained more silica gel than the other calcite structure.

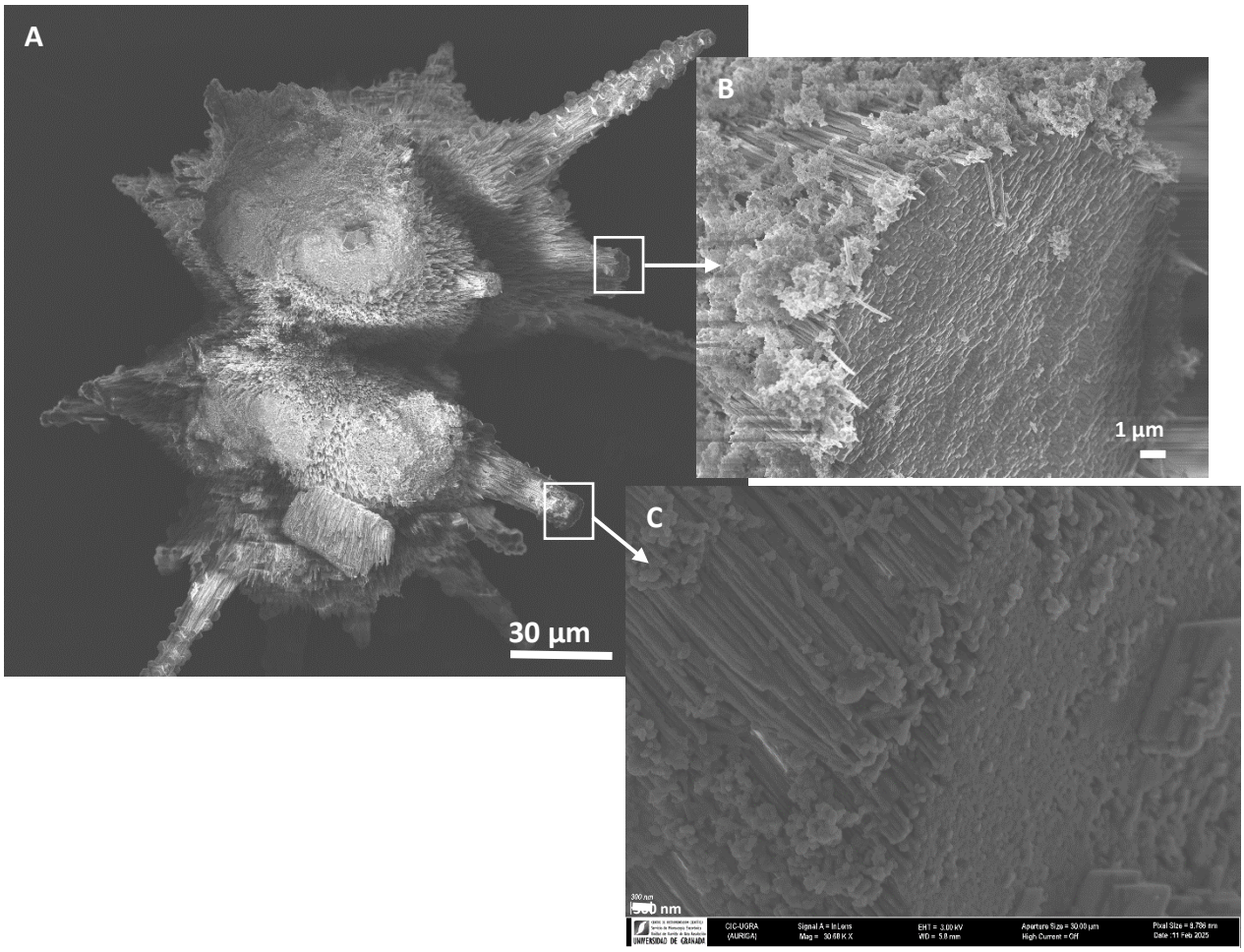

Figure 27 SEM image of a broken off section of a star-like calcite structure. The images of the broken off sections B and C allow to see the rod-like structuration of the calcite. Image C also show the trigonal symmetry of the calcite.

The difference in structuration between the aragonite biomorphs and the calcite structures could be the reason behind the ability of the aragonite to create smooth curve where has the calcite only forms wide sheets or long spikes. In the aragonite structures, the variation in size or width of the sheets leads to the curving of the arm, as the sheet are organised radially. In both calcite structures, the structuration is made of rods, growing following the same axis. In the case of the bi-conal structures, the rod also stacks radially, forming sheets, whereas in the case of the star-like structures, the rods form the spikes shooting out of the centre.

Another difference between the calcite and aragonite structures is the conservation of the trigonal geometry of the calcite, visible in the breaking points, while aragonite does not show any retention of the crystalline structure. This difference is most likely what allows aragonite to form structures with curvatures whereas calcite only forms straight spikes or flat sheets.

For both the aragonite biomorphs and the calcite stars, the structuration if the centre of the structure was not visible, as not of the structure broke in a way to show it. Additional study of those structure are thus necessary.

An interesting way to complement this analysis would be to use textural tomography.[20] This technique allows to recreate the polycrystalline structuration of

crystalline aggregate; by using X-ray diffraction. The object is divided into small enough volumes, so the microcrystal acts as a single crystal. By then analysing all the diffraction patterns, the microcrystalline structure of the object can be recreated. This would offer insight into the exact arrangement of the sheets of aragonite forming the biomorphs, or the exact arrangement of the calcite rods. The main drawback of this technique is the requirement of a synchrotron X-ray beam and the volume of data to treat requires high computational power.

6 Conclusion and outlook

In this work, we were able to concomitantly consistently crystalize aragonite and calcite at room temperature, in a silica gel. We highlighted the structural differences between the calcite and aragonite structures.

Calcite presents a constant morphological pattern throughout the different experiments. It first precipitates as classic calcite crystals, which then form aggregates. Calcite then precipitates in deformed crystals, with the silica blocking the faces and forcing the growth of the edges along the c axis. Finally, calcite forms polycrystalline aggregates, first composed of two cones attached by their summit, then spherical aggregates evolving into starlike structures.

Aragonite precipitates in a limited spatial region of the gel, and forms two main structures: highly twisting structures and longer, more expanding structures. The first forming at lower overall concentrations and the latter at higher overall concentrations. Additionally, we highlighted that aragonite seems to only form when the diffusion of the calcium in the gel is homogeneous, with higher concentrations of both carbonate and calcite (above 0.5mol/l) causing inhomogeneities and the absence of aragonite structures.

SEM analysis allowed us to highlight the differences between the micro-structuration of calcite and aragonite structures. Both type of calcite aggregates (double cone and starlike) are made of rods, arranged parallel and oriented toward the edge of the structure. We also find the trigonal geometry of calcite in the breaking points of the structures. Aragonite structures are made of sheets, stacked and oriented radially, forming the arms or the biomorphic structures. This arrangement could explain the ability of aragonite structures to form curvatures, by having smaller or thinner sheets on one side of the arm relative to the other.

To go further in the understanding of the formation of aragonite biomorphs, more factors can be studied, such as the starting pH or the temperature at which the experiment takes place. pH studies could give insight into the exact precipitation and formation mechanisms of both calcite and aragonite structures, allowing us to identify the chemical equilibria in action at the precipitation front or at the diffusion front. By modifying the temperature by heating, we could favour the formation of aragonite and the diffusion speed of calcite in the gel.

Further analysis of the aragonite structures by textural tomography would give us more insight into the exact internal structure of the biomorphs. This would help with the understanding of the formation process and the mechanisms creating the curved shapes of the biomorphs.

Lastly, once we have a strong understanding of the formation process in a pure system, we could add other molecules, either other metal ions or simple organic molecules. This would help with the understanding of the formation process in a more realistic environment and any shape or structural changes that might occur. Furthermore, the addition of simple organic molecules could help with the differentiation between living organism fossil and abiotic structure in fossil dating from the early stages of the apparition of life on Earth. Additionally, a way to control the shape and structure could open to nanotechnology applications, as a template to grow other structures or as a vessel to carry molecules.

7 Bibliography

[1] Kellermeier M.; Cölfen H.; García-Ruiz J-M., *Silica Biomorphs: Complex Biomimetic Hybrid Materials from "Sand and Chalk"*, Eur. J. Inorg Chem, 2012, 5123-5144

[2] Rouillard J, García-Ruiz J-M, Gong J, van Zuilen MA. *A morphogram for silica- witherite biomorphs and its application to microfossil identification in the early earth rock record*. Geobiology. 2018;16:279–296.

[3] Cameron E. M., Blum T. B., Cavosi A. J., Kitajima K., Nasdala L., orland I. J., Bonamici C. E., Valley J. W., *Evidence for oceans pre-4300 Ma confirmed by preserved igneous compositions in Hadean zircon* American Mineralogist, 2024, vol. 109, 1670–1681

[4]*,* Shang X., Huang R., Sun W., *An ammonia-methane dominated atmosphere in the Hadean Eon*, Solid Earth Sciences, 8, 2023, 191–194

[5] Rouillard J., García-Ruiz J-M., Gong J., van Zuilen M. A., *A morphogram for silica- witherite biomorphs and its application to microfossil identification in the early earth rock record*, Geobiology. 2018, 16:279–296

[6] Opel J., Wimmer F.P., Kellermeier M. Cölfen H. *Functionalisation of silica-carbonate biomorphs*, Nanoscale Horizons, 2016, Vol 1, 2, 144-149,

[7] Garcia Ruiz J.M., Carnerup A., Christy A. G., Welham N. J., Hyde S. T., *Morphology: An Ambiguous Indicator of Biogenicity*, ASTROBIOLOGY, Vol 2, 3, 2002

[8] Opel J., Brunner J., Zimmermanns R., Steegmans T., Strum E., Kellermeier M., Cölfen H., Garcia Ruiz J.M., *Symbiosis of Silica Biomorphs and Magnetite Mesocrystals*, Adv. Funct. Mater. 2019, 29, 1902047

[9] Menichetti A., Manzi J., Otálora F., Montalti M. and García-Ruiz J-M., *Morphological Sensitivity to pH of Silica and Chalk Nanocrystalline Self-Organized Biomorphs.* Small Sci.,2004, 4: 2400090.

[10] García-Ruiz J-M., van Zuilen M A., Bach W., *Mineral self-organization on a lifeless planet* , Physics of Life Reviews, 34–35 (2020) 62–82

[11] Barbosa N., Khakhula T., Brazard J., Adachi T. B. M., *Beauty and Complexity of Calcium Carbonate Precipitation: Optical Microscopy and insitu Raman Microspectroscopy Characterization*, Cryst. Growth Des., 2025 *25* (2), 210-224

[12] Lui D., Li P., He M., Shi Y., *Proteomic and functional analysis of the shell matrix proteins and the multifunctional Gh26 regulates biomineralization in the Gigantidas haimaensis*, International journal of Biological Macromolecules, 2025, 305

[13] Tarczewska A., Bielak K., Zoglowek, A. Sołtys K., Dobryszycki P., Ozyhar A., Rózycka M., *The Role of Intrinsically Disordered Proteins in Liquid–Liquid Phase Separation during Calcium Carbonate Biomineralization*, Biomolecules 2022, 12, 1266

[14] Hur S., Méthivier C., Wilson A., Salmain M., Boujday S., Miserez A., *Biomineralization in Barnacle Base Plate in Association with Adhesive Cement Protein*, *ACS Applied Bio Materials 2023 6 (9), 3423-3432*

[15] Zhang G., Verdugo-EscamillaC., Choquesillo-Lazarte D., García-Ruiz J-M., *Thermal assisted self-organization of calcium carbonate*, NATURE COMMUNICATIONS, 2018, 9:5221

[16] Zhang G., Morales J., García-Ruiz J-M., *Growth behaviour of silica/carbonate nanocrystalline composites of calcite and aragonite*, J. Mater. Chem. B, 2017

[17] Melero-Garcıa E., Santisteban-Bailon R., Garcıa-Ruiz J-M., *Role of Bulk pH during Witherite Biomorph Growth in Silica Gels*, Crystal Growth & Design, Vol. 9, No. 11, 2009

[18] Rruff database: Aragonite R040078 - RRUFF Database: Raman, X-ray, Infrared, and Chemistry

[19] Rruff database: Calcite R040170 - RRUFF Database: Raman, X-ray, Infrared, and Chemistry

[20] Frewein M.P.K., Mason J., Maier B., Cölfen H., Medjahed A., Burghammer M., Allain M., Grünewald T.A., *Texture tomography, a versatile framework to study crystalline texture in 3D*, IUCrJ, 2024, 11, 809–820

UNIVERSITÉ CATHOLIQUE DE LOUVAIN
Faculté des sciences
Place des sciences, 2 bte L6.06.01, 1348 Louvain-la-Neuve, Belgique | **www.uclouvain.be/sc**